



HAL
open science

APOLD1 loss causes endothelial dysfunction involving cell junctions, cytoskeletal architecture, and Weibel-Palade bodies, while disrupting hemostasis

Simon Stritt, Paquita Nurden, Alan T. Nurden, Jean-Francois Schved, Jean-Claude Bordet, Maguelonne Roux, Marie-Christine Alessi, David-Alexandre Tregouet, Taija Makinen, Muriel Giansily-Blaizot

► To cite this version:

Simon Stritt, Paquita Nurden, Alan T. Nurden, Jean-Francois Schved, Jean-Claude Bordet, et al.. APOLD1 loss causes endothelial dysfunction involving cell junctions, cytoskeletal architecture, and Weibel-Palade bodies, while disrupting hemostasis. *Haematologica*, 2023, 108 (3), pp.772-784. 10.3324/haematol.2022.280816 . hal-03691783

HAL Id: hal-03691783

<https://hal.science/hal-03691783>

Submitted on 9 Jun 2022

HAL is a multi-disciplinary open access archive for the deposit and dissemination of scientific research documents, whether they are published or not. The documents may come from teaching and research institutions in France or abroad, or from public or private research centers.

L'archive ouverte pluridisciplinaire **HAL**, est destinée au dépôt et à la diffusion de documents scientifiques de niveau recherche, publiés ou non, émanant des établissements d'enseignement et de recherche français ou étrangers, des laboratoires publics ou privés.



Distributed under a Creative Commons Attribution - NonCommercial 4.0 International License

APOLD1 loss causes endothelial dysfunction involving cell junctions, cytoskeletal architecture, and Weibel-Palade bodies, while disrupting hemostasis

by Simon Stritt, Paquita Nurden, Alan T. Nurden, Jean-François Schved, Jean-Claude Bordet, Maguelonne Roux, Marie-Christine Alessi, David-Alexandre Trégouët, Taija Mäkinen, and Muriel Giansily-Blaizot

Received: February 7, 2022.

Accepted: May 10, 2022.

Citation: Simon Stritt, Paquita Nurden, Alan T. Nurden, Jean-François Schved, Jean-Claude Bordet, Maguelonne Roux, Marie-Christine Alessi, David-Alexandre Trégouët, Taija Mäkinen, and Muriel Giansily-Blaizot. APOLD1 loss causes endothelial dysfunction involving cell junctions, cytoskeletal architecture, and Weibel-Palade bodies, while disrupting hemostasis. Haematologica. 2022 May 31. doi: 10.3324/haematol.2022.280816. [Epub ahead of print]

Publisher's Disclaimer.

E-publishing ahead of print is increasingly important for the rapid dissemination of science. Haematologica is, therefore, E-publishing PDF files of an early version of manuscripts that have completed a regular peer review and have been accepted for publication. E-publishing of this PDF file has been approved by the authors. After having E-published Ahead of Print, manuscripts will then undergo technical and English editing, typesetting, proof correction and be presented for the authors' final approval; the final version of the manuscript will then appear in a regular issue of the journal. All legal disclaimers that apply to the journal also pertain to this production process.

APOLD1 loss causes endothelial dysfunction involving cell junctions, cytoskeletal architecture, and Weibel-Palade bodies, while disrupting hemostasis

Authors : Simon Stritt^{1,*}, Paquita Nurden^{2,*}, Alan T. Nurden², Jean-François Schved³, Jean-Claude Bordet⁴, Maguelonne Roux⁵, Marie-Christine Alessi⁶, David-Alexandre Trégouët^{5,7}, Taija Mäkinen¹, Muriel Giansily-Blaizot³.

Affiliations: ¹Department of Immunology, Genetics and Pathology, Uppsala University, Uppsala, Sweden. ²Institut de Rythmologie et de Modélisation Cardiaque, Hôpital Xavier Arnoz, Pessac, France. ³Department of Biological Hematology, CHU Montpellier, Université de Montpellier, Montpellier, France. ⁴Hematology, Hospices civils de Lyon, Bron biology center and Hemostasis-Thrombosis, Lyon-1 University, Lyon, France. ⁵Laboratory of Excellence GENMED (Medical Genomics), Paris, France. ⁶Aix Marseille University, INSERM, INRAE, C2VN, Marseille, France. ⁷University of Bordeaux, INSERM, Bordeaux Population Health Research Center, U1219, Bordeaux, France.

Authors' contribution: SS, PN and TM designed experiments and analyzed data; SS, JCB and MGB performed experiments; MR, MCA, DAT and MGB performed genetic studies; PN, ATN, JFS, MCA, MGB enrolled the patients and performed clinical and biological follow up; SS, PN, ATN and TM wrote the manuscript with input from all other authors.

Running heads: APOLD1 regulates endothelial homeostasis

* **Corresponding authors:** Simon Stritt, PhD; Department of Immunology, Genetics and Pathology, Uppsala University, Uppsala, Sweden. E-mail: simon.stritt@igp.uu.se. Paquita Nurden, MD, PhD; Institut de Rythmologie et de Modélisation Cardiaque, Hôpital Xavier Arnoz, Pessac, France. E-mail: paquita.nurden@gmail.com.

Data sharing statement: Data is made available upon reasonable request.

Word count: Abstract word count: (225); **Text word count:** (4158/4000); **Number of figures and tables:** 6 figures; **Number of supplemental figures and tables:** 7 figures and 4 tables

Acknowledgements: We thank BioVis (Uppsala University) for electron microscopy analysis, CIQLE imaging center (Lyon-1 University) for immunogold labeling, Stephanie Burger-Stritt for help with experiments, Pauline Sauguet for collecting clinical data, as well as Henrik Ortsäter, Aissatu Mami Camara, Vanessa Ligonnet and Sofie Lunell-Segerqvist for technical assistance. We are grateful to Isabelle Cau and Alexandre Ranc for help with the t-PA ELISA. This work was supported by the Knut and Alice Wallenberg Foundation (2018.0218) and the Swedish Research Council (2020-02692) to TM. SS was supported by a research fellowship from the Deutsche Forschungsgemeinschaft (STR 1538/1-1) and a non-stipendiary long-term fellowship from the European Molecular Biology Organization (ALTF 86-2017). MR was supported by the GENMED Laboratory of Excellence on Medical Genomics, Agence Nationale de la Recherche (ANR-10-LABX-0013). The authors are grateful to the Fondation Maladies Rares for supporting the GIS Maladies Rares 2015 project entitled “Identification of new genes involved in platelet dysfunction”. DAT is partially supported by the *EPIDEMIO*-VT Senior Chair from the University of Bordeaux initiative of excellence IdEX.

Competing interests: The authors declare no competing financial interests.

ABSTRACT

Vascular homeostasis is impaired in various diseases thereby contributing to the progression of their underlying pathologies. The endothelial immediate early gene *Apolipoprotein L domain-containing 1* (*APOLD1*) helps regulate endothelial function. However, its precise role in endothelial cell (EC) biology remains unclear. We have immuno-localized *APOLD1* to EC cell contacts and to Weibel-Palade bodies (WPB) where it associates with von Willebrand factor (VWF) tubules. Silencing of *APOLD1* in primary human ECs disrupted the cell junction-cytoskeletal interface, thereby altering endothelial permeability accompanied by spontaneous release of WPB contents. This resulted in an increased presence of WPB cargoes, notably VWF and ANGPT2 in the extracellular medium. Autophagy flux, previously recognized as an essential mechanism for the regulated release of WPBs, was impaired in the absence of *APOLD1*. In addition, we report *APOLD1* as a candidate gene for a novel inherited bleeding disorder (IBD) across three generations of a large family associating an atypical bleeding diathesis with episodic impaired microcirculation. A dominant heterozygous nonsense *APOLD1*:p.R49* variant segregated to affected family members. Compromised vascular integrity resulting from an excess of plasma ANGPT2, and locally impaired availability of VWF may explain the unusual clinical profile of *APOLD1*:p.R49* patients. In summary, our findings identify *APOLD1* as an important regulator of vascular homeostasis and raise the need to consider testing of EC function in patients with IBDs without apparent platelet or coagulation defects.

INTRODUCTION

Regulation of vascular integrity and the prevention of excessive leakage of blood components are central for homeostasis and ensure proper organ function. Endothelial permeability varies between different vascular beds and is adjusted to the respective tissue functions, thereby allowing for gas exchange, regulation of extracellular fluid volume, osmolarity, pH as well as ion concentration. Breakdown of vascular integrity is a key feature of numerous pathologies not only including acute and chronic inflammatory diseases such as infections, asthma and arthritis, but also cancer and ischemic cardiovascular diseases with emphasis on myocardial infarction and stroke.^{1,2}

Vascular barrier function is mainly established by intercellular adherens and tight junctions between adjacent endothelial cells (ECs). The abundance and structural organization of junctional proteins such as claudin-5 (CLDN5) or vascular endothelial cadherin (VE-Cad; CDH-5) together with their modulation spatially and temporally determine vessel permeability. Stimulation of ECs with inflammatory mediators such as thrombin,³ or angiopoietin-2 (ANGPT2)⁴ results in EC activation, junction opening and the formation of intercellular gaps. Likewise, vascular injury or ischemia triggers EC activation and the release of bioactive mediators from Weibel-Palade bodies (WPBs) such as von Willebrand factor (VWF) and ANGPT2 thereby interfering with coagulation and also vessel permeability.⁵⁻⁷ In addition, endothelial activation is accompanied by the expression of immediate early genes such as *JUN* and *FOS* as well as the more recently identified *Apolipoprotein L domain-containing 1 (APOLD1)*.^{8,9} Platelet-, EC- and neuron-restricted APOLD1 has been implicated in angiogenesis as well as the regulation of endothelial permeability in mice in response to transient brain ischemia.⁹⁻¹² However, its precise role in EC biology as well as the involved molecular mechanisms remain unclear.

Using *in vitro* knockdown studies in human dermal blood ECs (HDBECs), we now define a role of APOLD1 in modulating the endothelial cytoskeleton, cell-cell junctions and WPB biology. Transfection of HDBECs with *APOLD1*-siRNA resulted in an increased release of WPBs through altered autophagy flux in favor of cargo secretion. Such findings may also have clinical implications, because an inherited *APOLD1*^{R49*} stop codon variant segregated to patients with bleeding of primarily

vascular origin within a large French family. Affected family members presented with a severe atypical bleeding diathesis despite unaltered platelet function that has remained undiagnosed during more than 20 years of extensive clinical and biological testing in expert centers including evaluations for platelet, coagulation and connective tissues defects. Treatment of bleeding during delivery or some surgeries was complicated not only because platelet transfusions failed to stop blood loss but also because the use of desmopressin to increase VWF secretion from ECs provoked a transiently impaired microcirculation. Therefore, our study highlights a new molecular pathway that may link defects primarily affecting ECs to a bleeding syndrome.

METHODS

Cell culture, preparation of platelets,¹³ immunolabeling of platelets and HDBECs,¹³ immunogold/transmission electron microscopy, immunoblotting, gene silencing, *in vitro* permeability assay, VWF, ANGPT1 and ANGPT2 ELISAs, image acquisition and image analysis^{14,15} were either performed according to the manufacturer's protocol or as previously described and are detailed in the Supplemental Information.

Whole exome and Sanger sequencing

Whole exome sequencing (detailed in Supplemental Information) identified two candidate variants in a large French family. Of these, *APOLD1*:p.R49* resulting from the combination of a common variant and a rare adjacent nucleotide substitution *in cis*, was a primary nonsense variant. Segregation analysis of both the common c.146G>A variant and the rare c.145C>T substitution in *APOLD1* was performed on DNA from 10 family members of three generations by Sanger sequencing. Blood samples of patients were obtained after informed consent in accordance with the declaration of Helsinki. Ethical approval was obtained in France from INSERM (RBM 04–14) for the national project “Network on the inherited diseases of platelet function and platelet production” and from the Montpellier local ethical committee (N° 202000352) for the project “Identification of new genes involved in platelet abnormal functions”.

Data presentation and statistical analysis

Data visualization and statistical testing was performed using GraphPad Prism 7. To compare between two means a nonparametric Wilcoxon-Mann-Whitney test was performed. For multiple comparisons a one-way ANOVA followed by Dunnett's multiple comparison test or a two-way ANOVA followed by Sidak's or Tukey's multiple comparison test was performed. *P*-values < 0.05 were considered as statistically significant (*), *p* < 0.05; (**), *p* < 0.01; (***), *p* < 0.001.

RESULTS

APOLD1 localizes to cell-cell junctions and WPBs

Given the endothelial and megakaryocyte/platelet-restricted expression of APOLD1,^{9,11} we first assessed its localization in primary HDBECs and human platelets. In agreement with previous reports, we detected APOLD1 at cell-cell junctions, defined by the presence of VE-Cad, of HDBECs in culture and in addition, we found a co-localization with the major WPB constituent VWF (Figure 1A). The WPB-specific localization of APOLD1 was further confirmed by immunogold electron microscopy (Figure 1B). While an occasional gold particle localized to the external membrane, the majority of gold particles were found inside the WPB suggesting an association of APOLD1 with the tubules of VWF (shown at high magnification in Figure 1B_{iii}). Of note, immunofluorescence labeling of platelets from human controls revealed localization of APOLD1 to α -granules and exclusion from δ -granules/lysosomes (Supplemental Figure 1A-B). Ultrastructurally, APOLD1 was occasionally found associated with the membrane of α -granules (Figure 1C_{i-iii}). In addition, APOLD1 immunogold labeling was also found to have an eccentric localization in the α -granule lumen (Figure 1C_{iv}), a finding previously described by Cramer *et al.*¹⁶ for platelet stored VWF in a manner resembling WPBs.

APOLD1 regulates the junctional and cytoskeletal architecture in ECs

To further study the function of APOLD1, we validated four short interfering RNAs (siRNA) to ablate *APOLD1* expression (Supplemental Figure 2A). Efficient silencing was confirmed by immunoblotting and immunolabeling (Supplemental Figure 2B-C). *APOLD1* silencing in HDBECs resulted in similar

cellular changes for all tested siRNAs (Supplemental Figure 2D). These changes were characterized by an increase in cell size as well as altered shape (Figure 2A-D) and were associated with EC junction dismantling evidenced by a reduction in the tight junction protein CLDN5, platelet-EC adhesion molecule 1 (PECAM1/CD31) as well as the reorganization of VE-Cad-positive adherens junctions (Figure 2A-B, E). Moreover, we also found a markedly enhanced fibronectin (FN) fibrillogenesis and actin stress fiber formation, reminiscent of EC activation (Figure 2A-B, E). Functionally, the observed alterations in the absence of *APOLD1* resulted in increased endothelial permeability to 40 kDa FITC-dextran, assessed by a transwell permeability assay (Figure 2F). Of note, 50% loss of *APOLD1* protein recapitulated the cellular defects observed upon efficient silencing (Supplemental Figure 2C and 3).

These results reveal a critical role of *APOLD1* in controlling EC junctions as well as cytoskeletal architecture and thereby in modulating endothelial permeability. Moreover, they suggest a critical threshold level of *APOLD1* to maintain endothelial homeostasis.

***APOLD1* interferes with EC storage organelle biology**

We next further explored the implication of *APOLD1* localization to endothelial WPBs. To this end we took a closer look at VWF, a major constituent of WPBs in ECs and present in platelet α -granules.¹⁷⁻¹⁹ Immunofluorescence labeling and immunoblotting revealed that *APOLD1*-silenced HDBECs in culture were almost devoid of VWF (Figure 3A-B). Changes in WPB content were not restricted to VWF but significantly, were also associated with a reduction in cellular ANGPT2 (Figure 3A-B), confirming impaired storage.²⁰ In agreement, we found markedly elevated levels of VWF and ANGPT2 in the supernatant of *APOLD1* siRNA-treated HDBECs as compared with controls (Figure 3C-D), excluding impaired protein production as the cause. Using transmission electron microscopy, we readily observed WPBs with the typical rod-shaped and striated ultra-structure in control cells (Figure 3E_i-F_{i-ii}). In contrast, we found that structurally abnormal organelles morphologically resembling autophagosomes with the typical isolation membrane predominated in *APOLD1* siRNA-treated HDBECs (Figure 3E_{ii}, 3F_{iii}). Immunogold labeling of VWF revealed that the remaining VWF in *APOLD1*-deficient HDBECs was mainly found in large vacuoles (Figure 3F_{iii}). An occasional WPB

still labeling for VWF was seen apparently releasing its cargo into a vacuole (Figure 3F_{iv}). Notably, control cells were devoid of these vacuoles and labeling for VWF was restricted to WPBs (Figure 3E, 3E_{i-ii}).

In summary these results suggest a role of APOLD1 in modulating endothelial WPB biology.

APOLD1 modulates WPB biology via secretory autophagy

Previous studies have identified a critical role of autophagy in WPB biogenesis and release.²¹ Given the excessive WPB release from HDBECs in the absence of APOLD1 (Figure 3A-D), we speculated that loss of APOLD1 would interfere with autophagy flux and thereby affect the secretory pathway. An increased expression of the autophagy markers SQSTM1 and LC3B in *APOLD1* siRNA-treated HDBECs was indeed reminiscent of an altered autophagy flux (Figure 4A-D). Furthermore, there was an increased co-localization of VWF with LC3B and the late endosomal/autophagosomal marker RAB7, whereas the association with SQSTM1 and the lysosomal marker LAMP1 were decreased (Figure 4A-F, Supplemental Figure 4). This was accompanied by a decreased ratio of mature and pro-VWF in APOLD1-deficient HDBECs revealing an abnormal autophagy-dependent proteolytic processing (Figure 5A-B). Significantly, blocking the fusion of autophagosomes with lysosomes, a final step of autophagy, with chloroquine resulted in an accumulation of lipidated LC3B-II and SQSTM1 in control HDBECs but did not affect the levels in *APOLD1*-silenced HDBECs (Figure 5A, C-D). All of these features have previously been associated with impaired autophagy flux likely in favor of increased priming of WPB for secretory autophagy.^{21,22} Therefore, we next silenced *autophagy related 5 (ATG5)* and *ATG7* genes which are critical for the initiation of autophagy and are implicated in WPB maturation as well as cargo release.²¹ Strikingly, simultaneous loss of *ATG5* or *ATG7* with *APOLD1* partially restored the presence of WPBs as compared with APOLD1-deficient HDBECs (Supplemental Figure 5A-C). Moreover, this led to a reduced release of WPBs evidenced by a decreased presence of VWF and ANGPT2 in the cell culture supernatant of *APOLD1/ATG5* and *APOLD1/ATG7* double-silenced HDBECs (Supplemental Figure 5D-F).

These findings reveal a role of APOLD1 in regulating WPB release through modulation of autophagy flux and suggest secretory autophagy as the primary route for the excessive WPB cargo release in the absence of APOLD1.

***APOLD1*^{R49*} associates with bleeding and vascular problems in a family with an inherited disorder**

Among the patient cohort studied by the French Reference Center for hemorrhagic syndromes was a large family with an inherited bleeding disorder (IBD) for which, despite extensive investigations over many years on coagulation factors and platelet biology in several expert centers (Supplemental Tables 1-3), no obvious cause could be identified. Based on these studies a vascular defect was suspected. The family history of the IBD extends over three generations (Figure 6A). The index patients are two sisters (pedigree member (PM) 4 and PM6; Figure 6A; Supplemental Table 1), now over seventy years old, who presented a severe atypical bleeding syndrome that was also present in their deceased father (PM1). In addition to the index patients, two of their children (PM9 and PM11), now adults, also suffer from excessive bleeding (Figure 6A; Supplemental Table 1). Their syndrome is characterized by severe spontaneous bleeding episodes during childhood, with extensive hemorrhage at menarche for the three affected women (PM4, PM6, PM9) that was difficult to control, and required hospitalization for PM9. Tranexamic acid was ineffective; different oral contraceptive therapies were tried for all of them but often non-tolerated, PM9 recently received leuprorelin injections.

PM6 and PM9 have also experienced periods of gastrointestinal (GI) bleeding. For PM6, this occurred in her sixties, was intermittent but not abundant. For PM9, GI bleeding was observed every 2-3 years during childhood but then stopped. Endoscopic investigations were not performed so that the presence of mild angiodysplasia cannot be excluded. Surgery (PM4, PM6, PM9, PM11) and childbirth (PM4, PM9) was on occasion accompanied by dramatic blood loss and platelet transfusions were ineffective. For PM9 bleeding during delivery was severe and persisted despite continuous transfusions of numerous packed red blood cells and platelet concentrates, but then progressively ceased. Tubal ligation was performed immediately after her first childbirth and for PM6 when she was 36 years old. Since middle age, no spontaneous bleeding has been observed for the patients. Another

characteristic of the three female index cases was the presence of microcirculatory problems (Supplemental Table 1). Noteworthy is that the use of vasodilators: piribedil (PM4, PM6), dihydroergocristine (PM9) for the treatment of Raynaud syndrome or retinal ischemia as well as aspirin (PM6, PM11) intake aggravated the bleeding tendency. Conversely, the use of desmopressin to increase VWF secretion from ECs in PM9 provoked a transiently impaired microcirculation evidenced by the appearance of livedo reticularis affecting her legs, due to which the treatment was discontinued (Supplemental Table 1).

Whole exome sequencing (WES) of DNA from PM4, PM6, PM9, PM12 and PM13 identified a heterozygous nonsense c.145_146delinsTA; p.R49* variant in *APOLD1* predicted to generate a premature stop codon at the early position 49 (detailed in Supplemental Information). Interestingly, the nonsense stop-gain p.R49* variant results from a combination *in cis* of the common c.146G>A; p.R49Q (rs4763876; minor allele frequency (MAF) 0.05292 Trans-Omics for Precision Medicine (TOPMed) and 0.07359 for the genome Aggregation Database (gnomAD); Polyphen: benign; SIFT: tolerated) and the rare missense c.145C>T; p.R49W (rs757476941; MAF 7.964×10^{-5} TOPMed and 6.637×10^{-5} for the gnomAD; Polyphen: probably damaging; SIFT: potentially deleterious) nucleotide substitution in *APOLD1* (Figure 6A, Supplemental Figure 6). Sanger sequencing of family members confirmed co-segregation of the R49* variant with the bleeding syndrome and additionally showed the presence of the common p.R49Q variant alone in asymptomatic relatives. Of note, PM4 was homozygous for the c.146G>A nucleotide substitution resulting in a compound heterozygous genotype of p.[R49Q];[R49*] (Figure 6A, Supplemental Figure 6). Except for the NM_006040:c.G1336T variant, which was not considered relevant on the basis of *HS3ST4* gene function, none of the other 17 candidate rare variants were predicted to be disease causing, and no other candidate mutations were present in any gene known to be associated with an inherited platelet or vascular derived bleeding disorder (Supplemental Table 4). Of note, the performed WES covered coding and flanking regions that were scrutinized for the presence of single nucleotide variations and insertions/deletions. More complex structural variations, or variations outside coding or flanking regions are not included in WES analyses.

Immunofluorescence labeling and immunoblot analysis revealed a ~50% reduction of APOLD1 in platelets from PM4 and PM6 as compared to healthy controls (Figure 6B-C), which is in agreement with the heterozygous transmission of the *APOLD1*^{R49*} variant (Figure 6A). Interestingly, despite the decreased labeling of α -granules by anti-APOLD1 antibodies (Figure 6D), granule numbers were normal (Figure 6D-E). Significantly, a decreased α -granule VWF content was noted when comparing the number of α -granules positive for VWF and P-selectin (Figure 6D, F, Supplemental Figure 7). This observation parallels the above-identified role of APOLD1 in endothelial VWF biology. In addition, we observed plasma VWF values to be either increased or at the high normal range (VWF:Ag: 186% for PM4; 127% for PM6; 157% for PM9; 186% for PM11; normal range <150%). It should be noted that the blood group of all patients is A (Supplemental Table 1). In addition, ANGPT2 plasma levels (2231 pg mL⁻¹ for PM4; 2490 pg mL⁻¹ for PM6; 1935 pg mL⁻¹ for PM11 normal range 1189 \pm 77 pg mL⁻¹) were increased in the patients studied, while the endothelium-stabilizing ANGPT1 (1191 pg mL⁻¹ for PM4; 1463 pg mL⁻¹ for PM6; 1135 pg mL⁻¹ for PM11; normal range 2893 \pm 457 pg mL⁻¹) concentration was decreased (Supplemental Table 2).

These results suggest *APOLD1* as a candidate gene for a novel EC-driven defect potentially underlying both the bleeding syndrome and microcirculatory problems in patients with an *APOLD1*^{R49*} variant.

DISCUSSION

Disintegration of the vascular barrier is a key feature of, and contributes to, the progression of various pathologies including cancer, chronic inflammatory conditions and cardiovascular diseases. Consequently, it is of much clinical interest to advance our understanding of the molecular machinery regulating endothelial integrity.^{1,2,23} Our study identifies the immediate early gene *APOLD1* as a modulator of endothelial homeostasis, regulating the junctional-cytoskeletal interface crucial for endothelial permeability and WPB biology through secretory autophagy. In addition, we describe the co-inheritance of a c.145_146delinsTA variant in *APOLD1* leading to a premature stop codon at p.R49* that segregates to affected members of a family with an unusual bleeding diathesis. Based on

their functions the other gene variants were not considered as candidates (Supplemental Table 4). Despite the reported expression of *APOLD1* in neurons,¹² there is no evidence of neurological abnormalities in affected patients, strongly suggesting a non-syndromic defect.

Our *in vitro* studies showed that *APOLD1* localizes to HDBEC cell junctions and to WPBs. Strikingly, loss of *APOLD1* disrupted the cytoskeletal and junctional organization of HDBECs with loss of the major junctional components VE-Cad and claudin-5,¹⁴ likely accounting for the increased vascular permeability and an altered central function of the EC cytoskeleton. However, much remains to be learned of the role of the associated cytoskeleton in maintaining EC morphology, junctional integrity and dynamics, as well as its potentially cell-type- and vascular bed-specific regulation.^{24–28} *APOLD1* silencing also perturbed WPB biology with an increased release of cargoes including VWF and ANGPT2^{17–20,29} due to impaired autophagy flux.³⁰ In support, biochemical and ultrastructural analyses revealed a reduced content in WPBs, an abnormal presence of autophagosomes as well as the detection of VWF inside large vacuoles in *APOLD1* siRNA-treated HDBECs. A seminal study by Torisu *et al.* identified a critical role of autophagy flux and *ATG5* as well as *ATG7* for basal WPB release.²¹ In our experiments the additive loss of *ATG5* or *ATG7* in *APOLD1*-silenced HDBECs partially restored the presence of WPB, confirming the participation of *APOLD1* in the process of autophagic WPB secretion.^{21,30} Globally, these results suggest the presence of a signaling cascade that regulates secretory autophagosome-trafficking of WPBs and our results suggest that *APOLD1* plays a central role therein.

Various cellular mechanisms can contribute to endothelial destabilization including kinase-/phosphatase-mediated phosphorylation/de-phosphorylation of junctional proteins or Rho GTPase signaling and the associated cytoskeletal alterations.²³ Of note, ANGPT2 has previously been shown to cause destabilization of the endothelium, promote inflammation, and to directly bind to and activate integrin $\alpha 5\beta 1$, thereby leading to junction dismantling.^{4,31–34} Consequently, it is tempting to speculate that the excessive WPB release may directly contribute to the junctional and cytoskeletal alterations as well as to the increased endothelial permeability of *APOLD1*-deficient HDBECs. In support of this, we observed an enhanced FN fibrillogenesis of *APOLD1* siRNA-treated cells, a process that involves ligand competent integrin $\alpha 5\beta 1$ in fibrillar adhesions.^{34,35}

Interestingly, up-regulation of *APOLD1* expression has been reported for patients under conditions of increased shear or cellular stress including inflammatory signals, physical exercise, and hypoxia.^{36,37} Further studies will be required to understand the consequences of such modifications including the activation of mechanosensory receptors, modifications of the vessel wall or WPB release. In an *APOLD1*-deficient mouse model, ischemic brain injury was evaluated because *APOLD1* initially named *vascular early response gene (VERGE)*, was recognized as an early gene expressed during ischemia.^{9,11} Loss of *Apold1* did not affect the infarct volume of the induced stroke, but resulted in decreased neurogenesis and angiogenesis during the following month.¹¹ More recently, a mild prothrombotic phenotype has been reported after laser-induced carotid vessel lesions in a similar model.³⁸ The mice had a somewhat shorter time to occlusion with increased tissue factor activity in the carotid artery and a reduced phosphorylation of the signaling protein, AKT in aortae. An enhanced aggregation of washed platelets was noted to collagen in the absence of *APOLD1*; however, the platelet aggregation responses in our family using platelet-rich plasma showed no significant changes. No data from additional models of thrombosis and hemostasis have been reported for *Apold1*^{-/-} mice. These published examples reflect the limited information available on the role of this gene and the consequences of its defects. Our *in vitro* studies in HDBECs showed an unexpected complex role of *APOLD1* in the regulation of vascular function and integrity through modulation of EC cytoskeleton and junctions as well as WPB biology. These findings expand the current understanding of *APOLD1* function in ECs. In the reported family with an unexplained complex phenotype combining severe bleeding and microvascular defects, WES, previously used to recognize new genes involved in unexplained inherited hematological disorders³⁹⁻⁴¹ identified *APOLD1* as the first candidate gene for the affected patients. A premature *APOLD1*^{R49*} stop codon variant arising from a co-inheritance of a potentially deleterious missense variant c.145C>T; p.R49W and a single nucleotide polymorphism (SNP) c.146G>A; p.R49Q co-segregated over three generations with a familial bleeding diathesis. This resulted in a truncated *APOLD1* protein lacking the three transmembrane domains and the coiled-coil domain that likely renders the protein dysfunctional. Importantly, the common c.146G>A; p.R49Q variant alone did not associate with a bleeding syndrome. In agreement with *APOLD1*^{R49*} heterozygosity, we observed approximately 50% levels of full length *APOLD1* protein in platelets of

PM4 and PM6. Furthermore, we found severe and progressive defects upon *APOLD1* silencing in primary HDBECs *in vitro*, suggesting a critical threshold level of APOLD1 to maintain normal EC physiology. A 50% reduction of APOLD1 in HDBECs significantly disrupted the cytoskeletal and junctional organization and affected WPB cargo content *in vitro*. This finding suggests that monoallelic defects of APOLD1 *in vivo* are compatible with a vascular defect. Of note, two other premature stop codon variants in *APOLD1* are present in the gnomAD database, however, their pathogenicity remains to be determined. It is important to note that disease-causing variants of MYH9-related disease, a well-studied bleeding disorder caused by rare monoallelic genetic variations, are also present in the gnomAD resource.⁴²

The unusual familial vascular syndrome that was not accompanied by prolonged classical bleeding times, with the patients refractory to platelet transfusions argues against a platelet disorder. Moreover, bleeding was observed in response to the use of vasodilators (PM4, PM5, PM9) indicating an unusual vascular fragility. It therefore appears that the APOLD1 defect in our patients affects critical aspects of the endothelium that favors the risk of hemorrhage, a process already described during inflammation,⁴³ and also observed in patients with hereditary hemorrhagic telangiectasia and cavernous malformations of the brain.^{44,45} The increased plasma levels of VWF and ANGPT2 detected in the tested patients suggests that the excessive release of WPBs identified *in vitro* for APOLD1-silenced HDBECs is also present *in vivo*. In addition, the patients had decreased plasma levels of ANGPT1. This causes a change in the balance between ANGPT1 and ANGPT2 a situation known to impair EC integrity and vascular stability through tyrosine kinase Tie2/Tie1 signaling.⁴⁶ Changes in the ratio of both these ligands are associated with various pathological states including inflammation and sepsis.⁴³ In von Willebrand Disease GI bleeding is frequently present resulting from reduced levels of VWF and increased ANGPT2 inducing proangiogenic dysplasia. The appearance of GI bleeds in the described family with an *APOLD1*^{R49*} variant raises questions on the underlying mechanisms and highlight the need for further investigations on the role of ANGPT1/ANGPT2 in the pathogenesis of lesion formation.

The predicted abnormalities of WPBs *in vivo* may contribute to the hemorrhagic syndrome during surgery. WPB defects are known to impair the local hemostatic response of the endothelium, even when plasma VWF levels are normal.^{47,48} An observed irregular bleeding during various surgical interventions could also reflect the tissue-specific expression of *APOLD1* in different vascular beds (https://endotheliomics.shinyapps.io/ec_atlas/).⁴⁹ It is known that the placenta contains high amounts of *APOLD1*, possibly explaining the important bleeding observed during delivery ([v21.proteinatlas.org;www.proteinatlas.org/ENSG00000178878-APOLD1/tissue](https://v21.proteinatlas.org/www.proteinatlas.org/ENSG00000178878-APOLD1/tissue)).⁵⁰ The transiently perturbed microcirculation in PM9 after administration of desmopressin to increase endothelial VWF secretion for the prevention of her hemorrhagic syndrome, further exemplifies the complexity of the phenotype of this family.

Beyond the classic forms of IBD associated with a platelet abnormality or VWF defects, many patients with a family history of bleeding remain undiagnosed. To date, analyzes on EC function are rarely performed, but should be considered in the future. To advance in this direction, panels designed for high-throughput sequencing could integrate genes involved in EC interactions and WPB function.⁵¹ We also anticipate that studies using patient-derived endothelial colony-forming cells (ECFC), also referred to as blood outgrowth endothelial cells, will be useful to explore the functional aspect of endothelial homeostasis and WPB biology for patients with an undiagnosed IBD. Up to now most of the studies employing ECFCs have focused on patients with von Willebrand disease. Finally, an improved understanding of the critical levels of predominantly EC-derived ANGPT2, t-PA and VEGF for the maintenance of vascular homeostasis will help to understand the implications of ECs in the pathogenesis of hemorrhagic syndromes.

In conclusion, we provide evidence that loss of *APOLD1* results in increased endothelial permeability and modified EC function with an excessive release of WPBs through secretory autophagy. Our findings strongly suggest that *APOLD1* modulates endothelial homeostasis with implications for vascular integrity and regulated WPB secretion. Given that *APOLD1* is an immediate early gene, its function might only fully come into play after traumatic vessel wall injury, or altered shear stress, e.g. in the context of ischemia, atherosclerosis as well as inflammatory settings, which lead to a boost of *APOLD1* transcription.^{9,36,37} Future studies with *Apold1*^{-/-} or knock-in mice as well as

patient-derived ECs are required to finally define more precisely the role of *APOLD1* in hemostasis and to further advance our understanding of the molecular functions of *APOLD1*.

REFERENCES

1. Hu X, De Silva TM, Chen J, Faraci FM. Cerebral Vascular Disease and Neurovascular Injury in Ischemic Stroke. *Circ Res*. 2017;120(3):449-471.
2. Murakami M, Simons M. Regulation of vascular integrity. *J Mol Med*. 2009;87(6):571-582.
3. Bogatcheva NV, Garcia JGN, Verin AD. Molecular mechanisms of thrombin-induced endothelial cell permeability. *Biochemistry (Mosc)*. 2002;67(1):75-84.
4. Hakanpaa L, Sipila T, Leppanen V-M, et al. Endothelial destabilization by angiopoietin-2 via integrin $\beta 1$ activation. *Nat Commun*. 2015;6:5962.
5. Starke RD, Paschalaki KE, Dyer CEF, et al. Cellular and molecular basis of von Willebrand disease: studies on blood outgrowth endothelial cells. *Blood*. 2013;121(14):2773-2784.
6. de Boer S, Eikenboom J. Von Willebrand Disease: From In Vivo to In Vitro Disease Models. *Hemasphere*. 2019;3(5):e297.
7. El-Mansi S, Nightingale TD. Emerging mechanisms to modulate VWF release from endothelial cells. *Int J Biochem Cell Biol*. 2021;131:105900.
8. Nagel T, Resnick N, Dewey CF, Gimbrone MA. Vascular endothelial cells respond to spatial gradients in fluid shear stress by enhanced activation of transcription factors. *Arterioscler. Thromb Vasc Biol*. 1999;19(8):1825-1834.
9. Regard JB, Scheek S, Borbiev T, et al. Verge: a novel vascular early response gene. *J Neurosci*. 2004;24(16):4092-4103.
10. Liu F, Turtzo LC, Li J, et al. Loss of vascular early response gene reduces edema formation after experimental stroke. *Exp Transl Stroke Med*. 2012;4(1):12.
11. Mirza MA, Capozzi LA, Xu Y, McCullough LD, Liu F. Knockout of vascular early response gene worsens chronic stroke outcomes in neonatal mice. *Brain Res Bull*. 2013;98:111-121.
12. Koshimizu H, Matsuoka H, Nakajima Y, et al. Brain-derived neurotrophic factor predominantly regulates the expression of synapse-related genes in the striatum: Insights from in vitro transcriptomics. *Neuropsychopharmacol Rep*. 2021;41(4):485-495.
13. Stritt S, Nurden P, Favier R, et al. Defects in TRPM7 channel function deregulate thrombopoiesis through altered cellular Mg(2+) homeostasis and cytoskeletal architecture. *Nat Commun*. 2016;7:11097.
14. Frye M, Dierkes M, Küppers V, et al. Interfering with VE-PTP stabilizes endothelial junctions in vivo via Tie-2 in the absence of VE-cadherin. *J Exp Med*. 2015;212(13):2267-2287.
15. Frye M, Taddei A, Dierkes C, et al. Matrix stiffness controls lymphatic vessel formation through regulation of a GATA2-dependent transcriptional program. *Nat Commun*. 2018;9(1):1511.
16. Cramer EM, Meyer D, le Menn R, Breton-Gorius J. Eccentric localization of von Willebrand factor in an internal structure of platelet alpha-granule resembling that of Weibel-Palade bodies. *Blood*. 1985;66(3):710-713.
17. Metcalf DJ, Nightingale TD, Zenner HL, Lui-Roberts WW, Cutler DF. Formation and function of Weibel-Palade bodies. *J Cell Sci*. 2008;121(Pt 1):19-27.

18. Rauch A, Wohner N, Christophe OD, et al. On the versatility of von Willebrand factor. *Mediterr J Hematol Infect Dis*. 2013;5(1):e2013046.
19. Randi AM, Smith KE, Castaman G. von Willebrand factor regulation of blood vessel formation. *Blood*. 2018;132(2):132-140.
20. Fiedler U, Scharpfenecker M, Koidl S, et al. The Tie-2 ligand angiopoietin-2 is stored in and rapidly released upon stimulation from endothelial cell Weibel-Palade bodies. *Blood*. 2004;103(11):4150-4156.
21. Torisu T, Torisu K, Lee IH, et al. Autophagy regulates endothelial cell processing, maturation and secretion of von Willebrand factor. *Nat Med*. 2013;19(10):1281-1287.
22. Wu Q, Hu Y, Jiang M, Wang F, Gong G. Effect of Autophagy Regulated by Sirt1/FoxO1 Pathway on the Release of Factors Promoting Thrombosis from Vascular Endothelial Cells. *Int J Mol Sci*. 2019;20(17):4132.
23. Claesson-Welsh L, Dejana E, McDonald DM. Permeability of the Endothelial Barrier: Identifying and Reconciling Controversies. *Trends Mol Med*. 2021;27(4):314-331.
24. Cavey M, Lecuit T. Molecular bases of cell-cell junctions stability and dynamics. *Cold Spring Harb Perspect Biol*. 2009;1(5):a002998.
25. Tzima E, del Pozo MA, Shattil SJ, Chien S, Schwartz MA. Activation of integrins in endothelial cells by fluid shear stress mediates Rho-dependent cytoskeletal alignment. *EMBO J*. 2001;20(17):4639-4647.
26. García Ponce A, Citalán Madrid AF, Vargas Robles H, et al. Loss of cortactin causes endothelial barrier dysfunction via disturbed adrenomedullin secretion and actomyosin contractility. *Sci Rep*. 2016;6:29003.
27. Sauteur L, Krudewig A, Herwig L, et al. Cdh5/VE-cadherin promotes endothelial cell interface elongation via cortical actin polymerization during angiogenic sprouting. *Cell Rep*. 2014;9(2):504-513.
28. Stehbens S, Wittmann T. Targeting and transport: how microtubules control focal adhesion dynamics. *J Cell Biol*. 2012;198(4):481-489.
29. Spiel AO, Gilbert JC, Jilma B. von Willebrand factor in cardiovascular disease: focus on acute coronary syndromes. *Circulation*. 2008;117(11):1449-1459.
30. New J, Thomas SM. Autophagy-dependent secretion: mechanism, factors secreted, and disease implications. *Autophagy*. 2019;15(10):1682-1693.
31. Felcht M, Luck R, Schering A, et al. Angiopoietin-2 differentially regulates angiogenesis through TIE2 and integrin signaling. *J Clin Invest*. 2012;122(6):1991-2005.
32. Hakanpaa L, Kiss EA, Jacquemet G, et al. Targeting β 1-integrin inhibits vascular leakage in endotoxemia. *Proc Natl Acad Sci U S A*. 2018;115(28):E6467-E6476.
33. Saharinen P, Eklund L, Alitalo K. Therapeutic targeting of the angiopoietin-TIE pathway. *Nat Rev Drug Discov*. 2017;16(9):635-661.
34. Clark K, Pankov R, Travis MA, et al. A specific α 5 β 1-integrin conformation promotes directional integrin translocation and fibronectin matrix formation. *J Cell Sci*. 2005;118(Pt 2):291-300.
35. Geiger B, Spatz JP, Bershadsky AD. Environmental sensing through focal adhesions. *Nat Rev Mol Cell Biol*. 2009;10(1):21-33.
36. Zhou L, Wang LM, Song HM, et al. Expression profiling analysis of hypoxic pulmonary disease. *Genet Mol Res*. 2013;12(4):4162-4170.
37. Simonsen ML, Alessio HM, White P, Newsom DL, Hagerman AE. Acute physical activity effects on cardiac gene expression. *Exp Physiol*. 2010;95(11):1071-1080.
38. Diaz-Cañestro C, Bonetti NR, Wüst P, et al. Apold1 deficiency associates with increased arterial thrombosis in vivo. *Eur J Clin Invest*. 2020;50(2):e13191.
39. Nurden AT, Nurden P. High-throughput sequencing for rapid diagnosis of inherited platelet disorders: a case for a European consensus. *Haematologica*. 2018;103(1):6-8.

40. Bastida JM, Lozano ML, Benito R, et al. Introducing high-throughput sequencing into mainstream genetic diagnosis practice in inherited platelet disorders. *Haematologica*. 2018;103(1):148-162.
41. Heremans J, Freson K. High-throughput sequencing for diagnosing platelet disorders: lessons learned from exploring the causes of bleeding disorders. *Int J Lab Hematol*. 2018;40 Suppl 1:89-96.
42. Bury L, Megy K, Stephens JC, et al. Next-generation sequencing for the diagnosis of MYH9-RD: Predicting pathogenic variants. *Hum Mutat*. 2020;41(1):277-290.
43. Goerge T, Ho-Tin-Noe B, Carbo C, et al. Inflammation induces hemorrhage in thrombocytopenia. *Blood*. 2008;111(10):4958-4964.
44. Mallet C, Lamribet K, Giraud S, et al. Functional analysis of endoglin mutations from hereditary hemorrhagic telangiectasia type 1 patients reveals different mechanisms for endoglin loss of function. *Hum Mol Genet*. 2015;24(4):1142-1154.
45. Lopez-Ramirez MA, Pham A, Girard R, et al. Cerebral cavernous malformations form an anticoagulant vascular domain in humans and mice. *Blood*. 2019;133(3):193-204.
46. Bilimoria J, Singh H. The Angiopoietin ligands and Tie receptors: potential diagnostic biomarkers of vascular disease. *J Recept Signal Transduct Res*. 2019;39(3):187-193.
47. James AH, Eikenboom J, Federici AB. State of the art: von Willebrand disease. *Haemophilia*. 2016;22 Suppl 5:54-59.
48. Schillemans M, Kat M, Westeneng J, et al. Alternative trafficking of Weibel-Palade body proteins in CRISPR/Cas9-engineered von Willebrand factor-deficient blood outgrowth endothelial cells. *Res Pract Thromb Haemost*. 2019;3(4):718-732.
49. Kalucka J, de Rooij LPMH, Goveia J, et al. Single-Cell Transcriptome Atlas of Murine Endothelial Cells. *Cell*. 2020;180(4):764-779.e20.
50. Uhlén M, Fagerberg L, Hallström BM, et al. Proteomics. Tissue-based map of the human proteome. *Science*. 2015;347(6220):1260419.
51. Kat M, Margadant C, Voorberg J, Bierings R. Dispatch and delivery at the ER-Golgi interface: how endothelial cells tune their hemostatic response. *FEBS J*. 2022 Mar 5. [Epub ahead of print]
52. Gustafsson N, Culley S, Ashdown G, et al. Fast live-cell conventional fluorophore nanoscopy with ImageJ through super-resolution radial fluctuations. *Nat Commun*. 2016;7:12471.

FIGURE LEGENDS

Figure 1: APOLD1 localizes to endothelial cell-cell junctions and von Willebrand factor storage organelles.

A) Cultured human dermal blood endothelial cells (HDBECs) were immunolabeled for Apolipoprotein L domain-containing 1 (APOLD1; green (SRRF processed⁵²)), von Willebrand factor (VWF; cyan), vascular endothelial cadherin (VE-Cad; magenta), F-actin (gray), and nuclei were highlighted with DAPI (blue) and subsequently analyzed by confocal microscopy. Scale bar, 10 μ m.

B) Immunogold labeling of adherent HDBECs for APOLD1 and subsequent electron microscopic analysis revealed localization to cell-cell contacts (i, arrowheads) and Weibel Palade bodies (ii-iii, arrows). Scale bars, 100 nm. Images in **A** and **B** are representative of at least three independent experiments. **C)** Immunogold labeling of resting human control platelets reveals APOLD1 localized to the membranes of α -granules (ii-iii) and to have an eccentric localization in the granule lumen, suggesting a possible association with VWF (iv). Of note, APOLD1 was not detected on the platelet surface. Scale bars, 200 nm (i) or 50 nm (ii-iv). Images are representative of one experiment.

Figure 2: APOLD1 silencing alters cytoskeletal and junctional organization of HDBECs. A-B)

APOLD1 silencing in HDBECs alters the organization of cell-cell junctions (claudin 5, CLDN5; vascular endothelial cadherin, VE-Cad; platelet-endothelial cell adhesion molecule 1, PECAM1/CD31) as well as cytoskeletal architecture and leads to increased fibronectin (FN) fibrillogenesis. Arrowheads in **A** highlight disrupted/CLDN5 negative junctions. Scale bars, 25 μ m. Images are representative of three independent experiments. **C-D)** Lack of *APOLD1* results in increased HDBEC size and altered shape (AR, Aspect ratio = major axis : minor axis). Box plots display first and third quartiles, and whiskers mark minimum and maximum values unless exceeding 1.5 times the interquartile range of at least 150 cells per group from three independent experiments; symbols represent outliers, and the horizontal line denotes the median. **E)** Image analysis revealed reduced immunolabeling intensities of the junctional proteins claudin 5 (CLDN5) and PECAM1/CD31, alterations of VE-Cad distribution as well as enhanced FN fibrillogenesis and actin stress fiber formation, which is reminiscent of endothelial cell activation leading to an increased **(F)**

endothelial permeability (40 kDa dextran-FITC). Data in **E** represent mean \pm s.d. Each symbol in **E**

represents the average of at least 100 cells from an individual experiment. Pooled data from at least four experiments is displayed. Each symbol in **F** represents one replicate from three independent experiments. Wilcoxon-Mann-Whitney test, *** $P < .001$.

Figure 3: APOLD1 modulates Weibel-Palade body biology. **A-C)** *APOLD1* silencing results in a loss of the major Weibel-Palade body constituent von Willebrand factor (VWF) as well as angiopoietin 2 (ANGPT2) as revealed by **(A)** immunolabeling and **(B)** immunoblotting with subsequent densitometric quantification of VWF and ANGPT2 levels relative to GAPDH in total cell lysates of control and *APOLD1* siRNA-treated HDBECs. Scale bars, 25 μm . Images and immunoblots are representative of at least three independent experiments. Each symbol in **B** represents one experiment and horizontal lines denote mean \pm s.d. Wilcoxon-Mann-Whitney test, *** $P < .001$. **C-D)** VWF and ANGPT2 content in the supernatant of control and *APOLD1* siRNA-treated HDBECs determined by ELISA. Each symbol represents an individual sample and horizontal lines denote mean \pm s.d. Pooled data from four independent experiments is displayed. Wilcoxon-Mann-Whitney test, *** $P < .001$. **E)** Electron microscopic images of Weibel-Palade bodies (WPB) in control siRNA-treated HDBECs (i) and autophagosomes (asterisks) with a developing isolation membrane (arrows) in *APOLD1*-silenced HDBECs (ii). M, mitochondria. Scale bars, 200 nm. Electron microscopic images are representative of three independent experiments. **F)** Immunogold (5 or 10 nm gold particles) labeling of VWF highlights WPBs with the typical striated rod-shaped structure in control cells (i-ii) while in *APOLD1*-silenced HDBECs (iii-v) VWF labeling was detected in vacuoles containing amorphous material (iii, arrowheads) and into which WPBs release their cargoes (arrows in iv). Scale bars, 50 nm (i-ii, iv) or 100 nm (iii). Images are representative of three independent experiments.

Figure 4: Increased WPB release likely occurs via dysfunctional autophagy flux. **A-F)** Immunolabeling and subsequent image analysis of control or *APOLD1* siRNA-treated HDBEC monolayers reveals increased expression of autophagy markers **(A, C)** SQSTM1 and **(B, D)** LC3B in the absence of *APOLD1*. VWF co-localized to a lesser extent to **(A, E)** SQSTM1 but showed an increased localization to **(B, F)** LC3B-positive vesicles upon *APOLD1* silencing. Each symbol in **C-F**

represents one analyzed ($n \geq 4$) image. Horizontal lines represent mean \pm s.d. Wilcoxon-Mann-Whitney test, $***P < .001$. Images are representative of at least three independent experiments. Scale bars, 10 μm .

Figure 5: Impaired proteolytic processing of VWF upon loss of APOLD1. **A)** Immunoblotting of lysates from mock and chloroquine-treated (25 μM for 12 h) control or *APOLD1* siRNA-treated HDBECs with subsequent densitometric quantification of **(B)** proteolytic VWF processing, **(C)** SQSTM1 and **(D)** LC3B I/II expression. Immunoblots are representative of at least three independent experiments. Bar graphs in **B-D** represent mean \pm s.d. Two-way ANOVA followed by Sidak's multiple comparison test, $***P < .001$.

Figure 6: APOLD1 is a candidate gene for a bleeding diathesis. **A)** Pedigree of the family with a variant in *APOLD1*. The red filled symbols indicate a bleeding diathesis co-segregating with a nonsense c.145_146delinsTA variant in *APOLD1*, resulting in a premature stop codon at arginine 49 (R49*). Pedigree members (PM) 7 and 13 only carry the more frequent single base pair substitution c.G146A in *APOLD1* (R49Q) which was not associated with a bleeding syndrome. The hashtags indicate patients studied by whole exome sequencing. The other family members have been subjected to Sanger sequencing of *APOLD1*. Green filled symbols indicate occurrence of impaired microcirculation and yellow filled symbols of drug-associated bleeding. **B)** Resting poly-L-lysine immobilized platelets of healthy control and pedigree members (PM) 4 and 6 were stained for APOLD1 (magenta), CD41 (cyan) and F-actin (gray). Scale bars, 3 μm . **C)** APOLD1 protein expression was analyzed by immunoblotting and densitometric quantification relative to GAPDH of platelet lysates from two unrelated healthy controls as well as PM4 and PM6. The antibody was directed against aa139-192 and only detects full length APOLD1. Immunoblots are representative of 3 experiments. Data represent mean \pm s.d. **D)** Resting platelets of control or PM4 and PM6 were labeled for CD62 (P-selectin, green; α -granule marker), von Willebrand factor (VWF, magenta; α -granule marker), and CD63 (granulophysin, cyan; δ -granule/lysosome marker). F-actin is highlighted in grey.

Scale bars, 3 μm . **E-F)** Quantification of CD62P-, VWF- and CD63-positive granules per platelet from healthy control, PM4 and PM6. Box plots display first and third quartiles, and whiskers mark minimum and maximum values unless exceeding 1.5 times the interquartile range of at least 100 cells per group; symbols represent outliers, and the horizontal line denotes the median. Results were analyzed by one-way ANOVA followed by Dunnett's multiple comparisons test, *** $P < .001$.

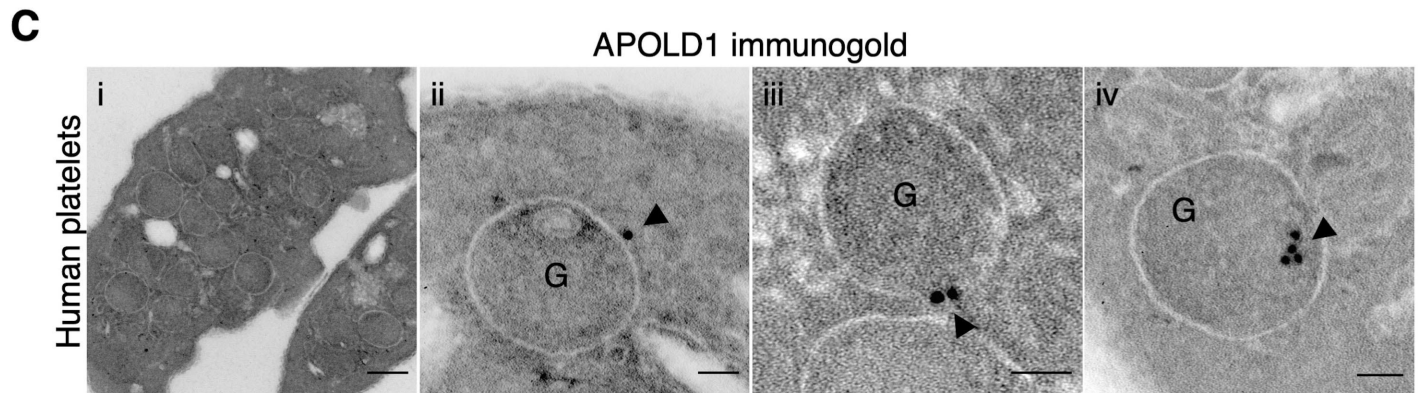
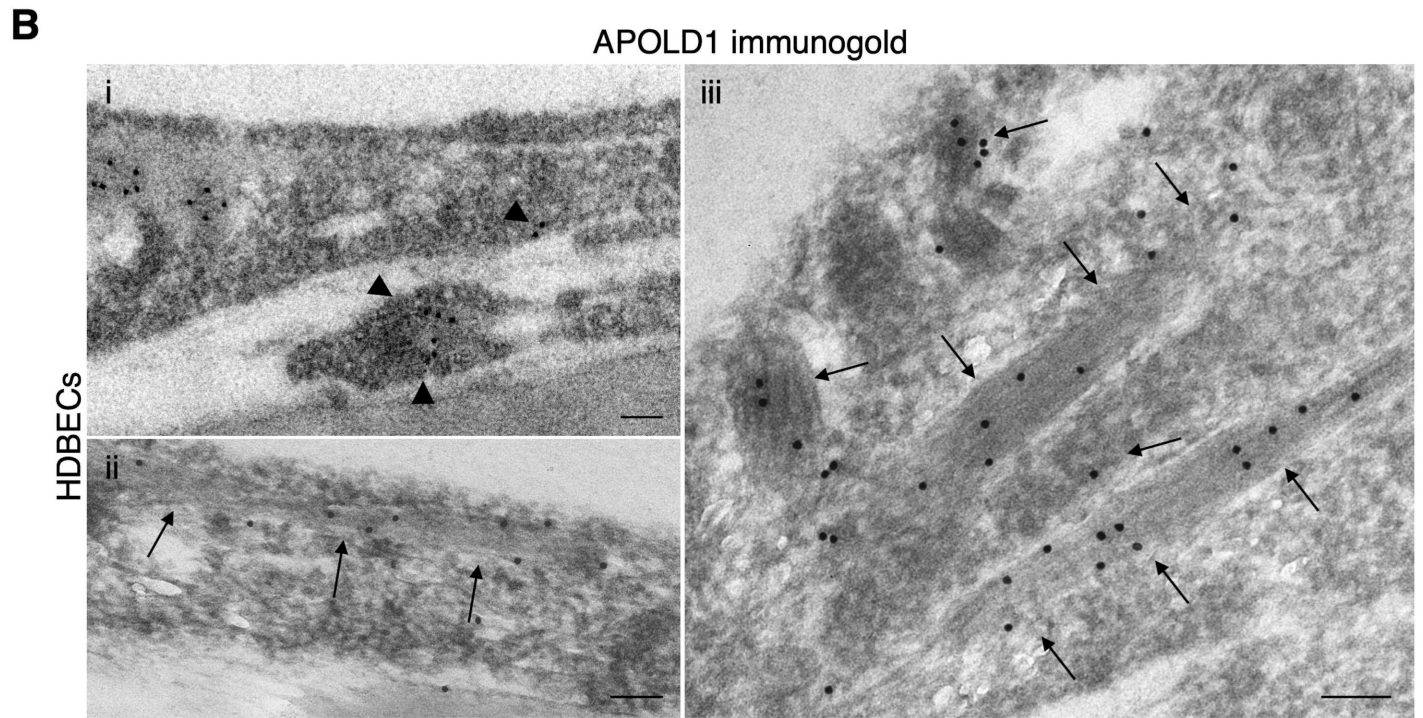
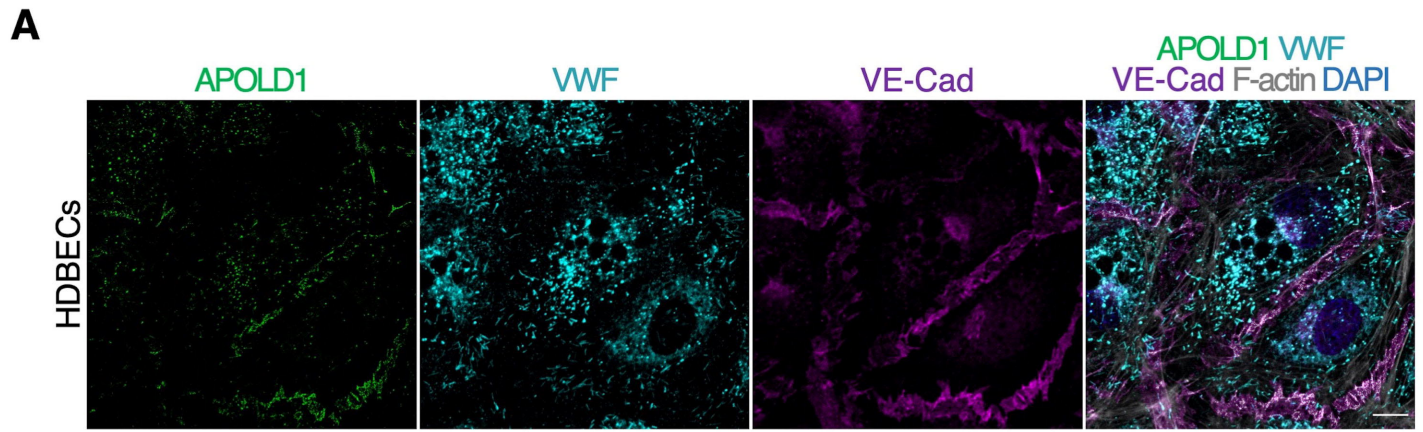
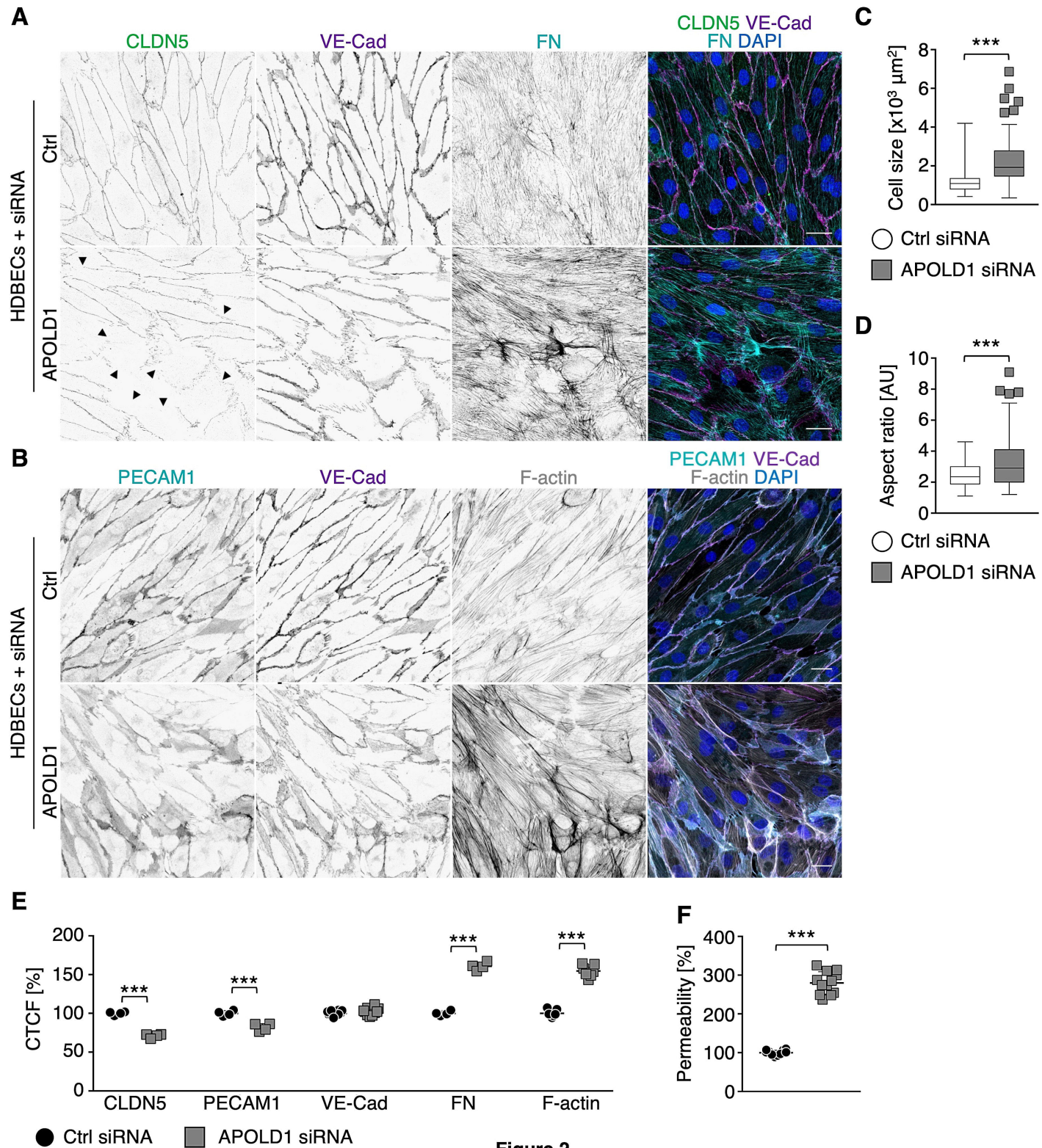


Figure 1



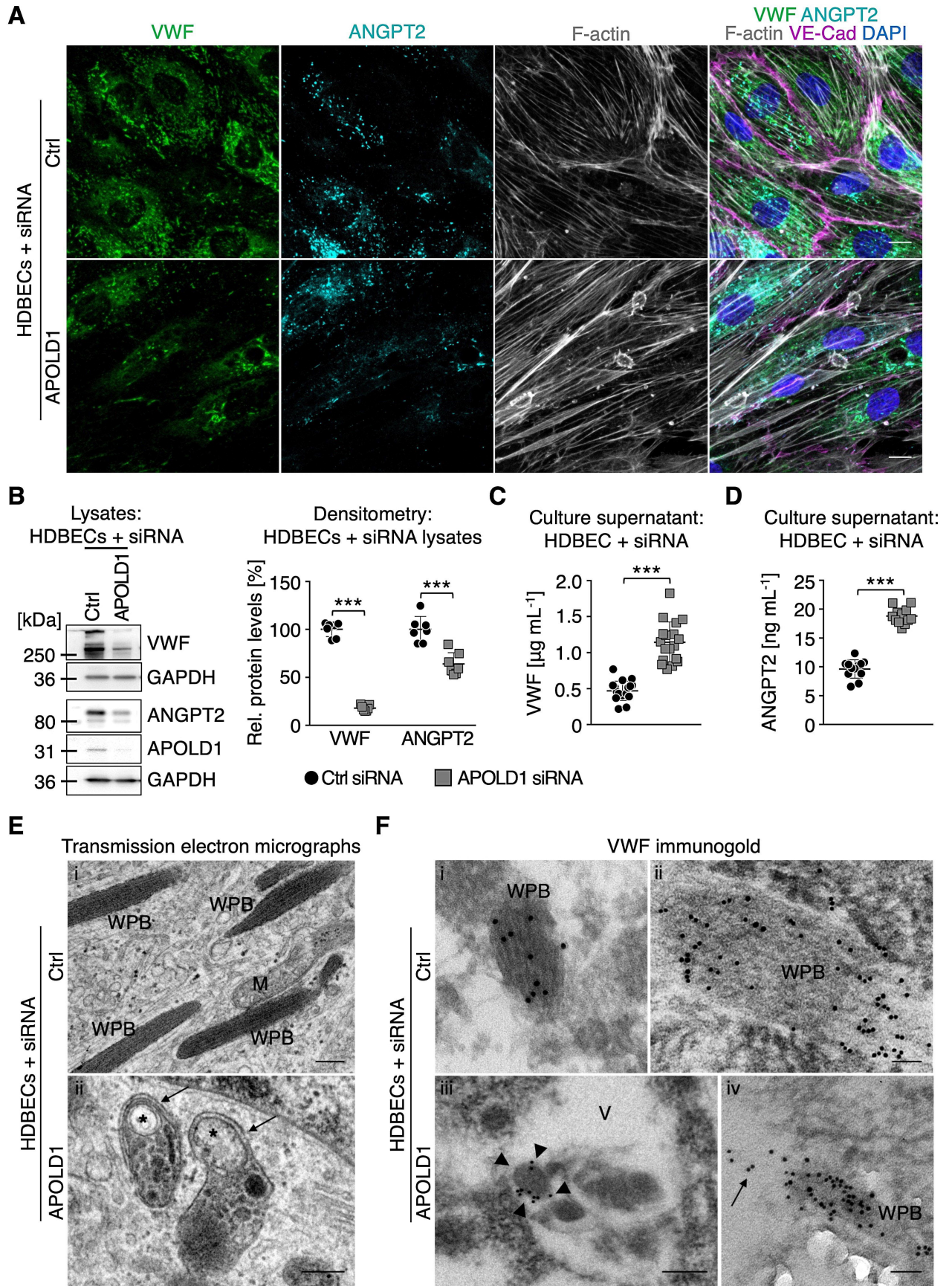


Figure 3

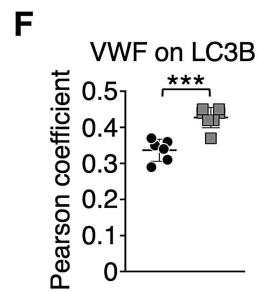
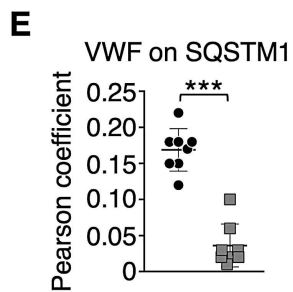
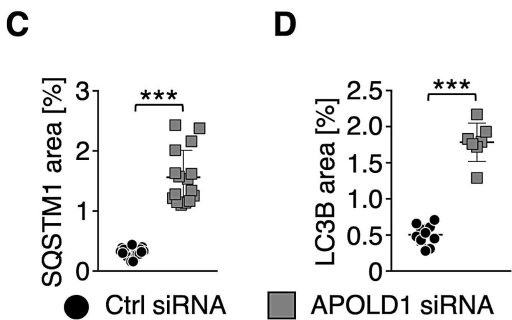
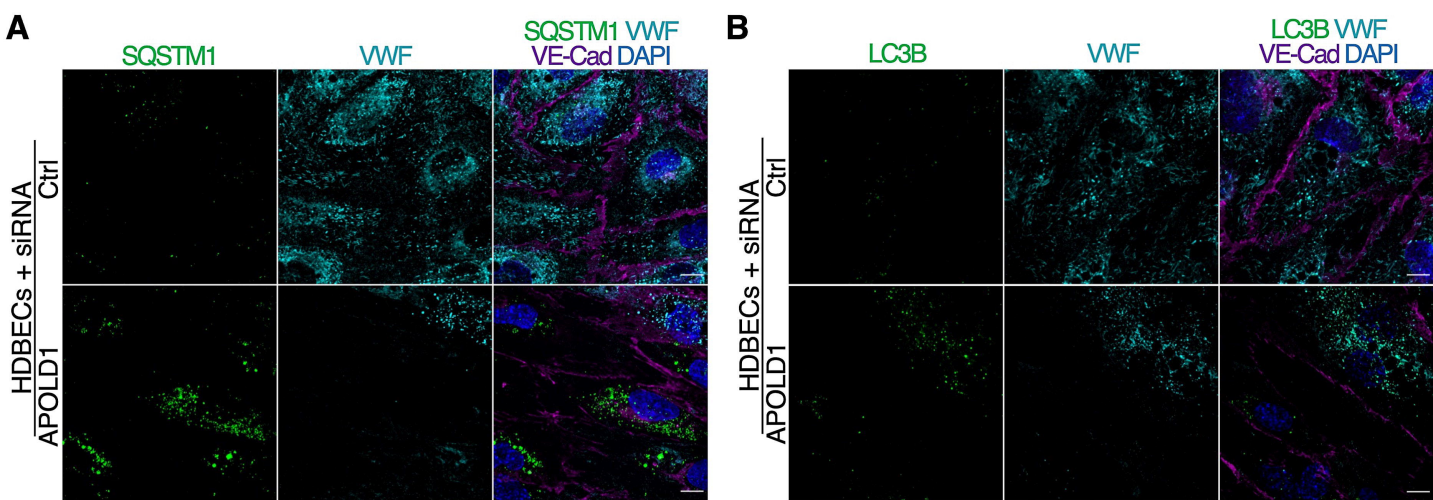


Figure 4

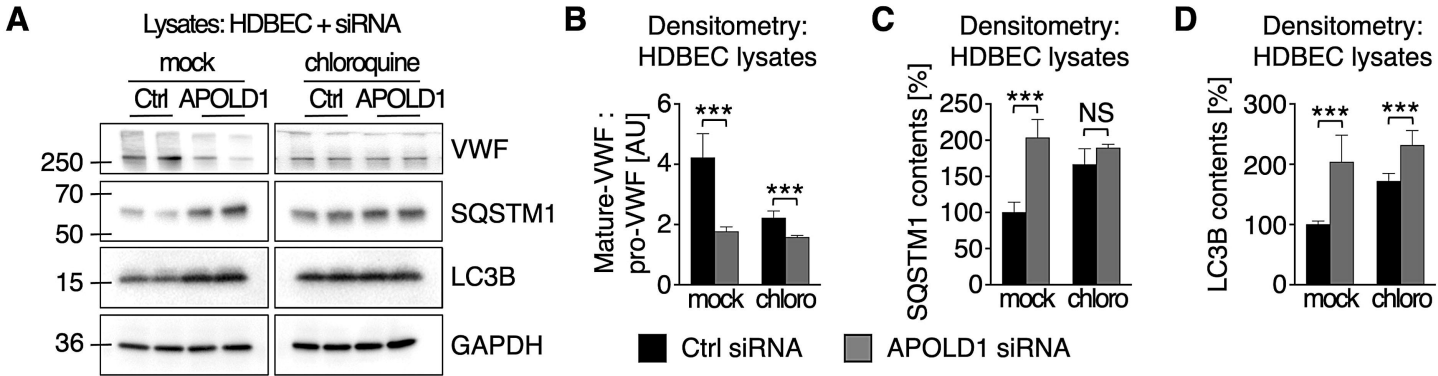


Figure 5

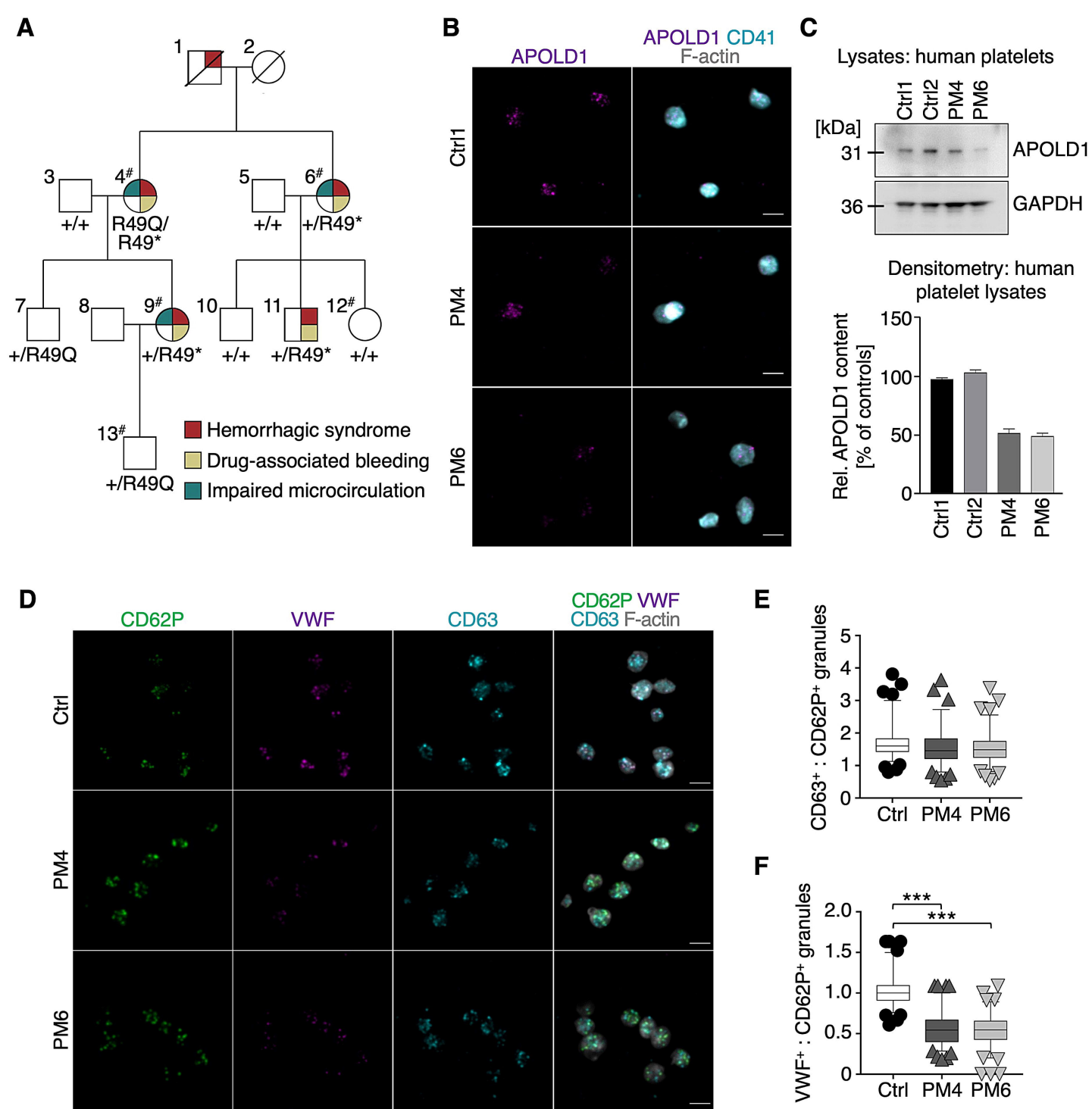


Figure 6

SUPPLEMENTAL METHODS

Cell culture

Primary human dermal microvascular endothelial cells (HDMECs) from juvenile foreskin were obtained from PromoCell (C12210). Cells were maintained in cell culture dishes coated with $0.2 \mu\text{g cm}^{-2}$ bovine fibronectin (F1141, Sigma-Aldrich) supplied with complete Endothelial Cell Growth Medium 2 (ECGMV2; C-22022, PromoCell). At 90% confluency HDMECs were gently detached with Accutase (A6964, Sigma-Aldrich), washed with complete medium and incubated for 45 min at 4°C with rat anti-human podoplanin antibody-coated (NZ-1, 14-9381-82, Thermo-Fisher Scientific, $7 \mu\text{g}$ per 100 mm dish) Dynabeads (11035, Thermo-Fisher Scientific) and subsequently separated into bead-bound lymphatic and unbound blood ECs by magnetic sorting. Purity was assessed by immunolabeling for PDPN and PROX1. Cells were maintained at 37°C and 5% CO_2 . Purified human dermal blood ECs (HDBECs) were maintained in cell culture dishes coated with $0.2 \mu\text{g cm}^{-2}$ bovine fibronectin (F1141, Sigma-Aldrich) in complete Endothelial Cell Growth Medium 2 (ECGMV2; C-22022, PromoCell) and passaged at 90% confluency using Trypsin-EDTA (25300-054, Thermo-Fisher Scientific). For the indicated experiments fusion of lysosomes and autophagosomes was inhibited by treatment with $25 \mu\text{M}$ chloroquine (dissolved in ddH_2O ; C6628, Sigma-Aldrich).

Platelet preparation

Blood samples of patients were obtained after informed consent in accordance with the declaration of Helsinki. Ethical approval was obtained in France from INSERM (RBM 04–14) for the national project ‘Network on the inherited diseases of platelet function and platelet production’. Fresh blood samples of patients and healthy volunteers were collected in 1/10 volume of acid-citrate-dextrose and centrifuged for 10 min at 200 g. Platelet-rich plasma (PRP) was collected, supplemented with $3 \mu\text{L}$ of apyrase (0.02 U mL^{-1} , A6410, Sigma-Aldrich) and $5 \mu\text{L}$ Prostacyclin I_2 (PGI_2) ($0.1 \mu\text{g mL}^{-1}$, P6188, Sigma-Aldrich) per mL PRP. Before adherence to poly-L-lysine (PLL, P8920, Sigma-Aldrich)-coated slides, platelets were pelleted by centrifugation for 10 min at 800 g and washed twice with Tyrode-N-2-hydroxyethyl-piperazine-N’2-ethanesulfonic acid (HEPES) buffer (134 mM NaCl, 0.34 mM Na_2HPO_4 , 2.9 mM KCl, 12 mM NaHCO_3 , 5 mM HEPES, 5 mM glucose, 0.35% bovine serum albumin (BSA), pH 7.4) containing $2 \mu\text{L mL}^{-1}$ apyrase and $5 \mu\text{L mL}^{-1}$ PGI_2 . Subsequently samples were resuspended at 2 x

10^5 platelets μL^{-1} in Tyrode-HEPES buffer containing $2 \mu\text{L mL}^{-1}$ apyrase and $5 \mu\text{L mL}^{-1}$ PGI₂ and were allowed to rest for 30 min at 37 °C prior to being used in experiments.

Immunolabeling of resting platelets and HDBECs

For platelet studies coverslips were coated with PLL overnight at 4 °C. Platelets were allowed to adhere for 20 minutes, fixed in PHEM buffer (60 mM piperazine-N,N-bis-2-ethanesulfonic acid (PIPES), 25 mM HEPES, 10 mM EGTA, 2 mM MgCl₂, pH 6.9) supplemented with 4% PFA, permeabilized and blocked with 0.1% IGEPAL CA-630 (I8896, Sigma-Aldrich), 3% bovine serum albumin (BSA, A3295, Sigma-Aldrich) in PBS and stained with the indicated primary antibodies. HDBECs were processed in a similar manner, but were grown on $0.2 \mu\text{g cm}^{-2}$ bovine fibronectin-coated (F1141, Sigma-Aldrich) coverslips. The following primary antibodies were used for immunofluorescence staining: rat anti-CD41 ($3.33 \mu\text{g mL}^{-1}$, 14-0411-82 (MWReg30), Thermo-Fisher Scientific), rabbit anti-APOLD1 C-term ($5.0 \mu\text{g mL}^{-1}$, ab105079, Abcam), rabbit anti-VWF ($3.33 \mu\text{g mL}^{-1}$, A0082, DAKO), goat anti-VE-Cad ($0.67 \mu\text{g mL}^{-1}$, sc-6458 (C-19), Santa-Cruz Biotechnology), rabbit anti-claudin 5 ($3.33 \mu\text{g mL}^{-1}$, 34-1600, Thermo-Fisher Scientific), mouse anti-FN ($5.0 \mu\text{g mL}^{-1}$, F6140, Sigma-Aldrich), mouse anti-VE-Cad ($0.67 \mu\text{g mL}^{-1}$, sc-9989 (F-8), Santa-Cruz Biotechnology), mouse anti-CD31 ($2.5 \mu\text{g mL}^{-1}$, M0823, DAKO), goat anti-ANGPT2 ($2.5 \mu\text{g mL}^{-1}$, AF623, R&D Systems), mouse anti-VWF ($0.67 \mu\text{g mL}^{-1}$, sc-53466 (F-8/86), Santa-Cruz Biotechnology), mouse anti-CD62P ($5.0 \mu\text{g mL}^{-1}$, sc-8419 (CTB201), Santa-Cruz Biotechnology), mouse anti-CD63 ($3.33 \mu\text{g mL}^{-1}$, 10628D (Ts63), Thermo-Fisher Scientific), mouse anti-LAMP1 ($5.0 \mu\text{g mL}^{-1}$, #15665 (D4O1S), Cell Signaling Technology), mouse anti-RAB7 ($5.0 \mu\text{g mL}^{-1}$, #95746 (E9O7E), Cell Signaling Technology), mouse anti-LC3B ($5.0 \mu\text{g mL}^{-1}$, #83506 (E5Q2K), Cell Signaling Technology), and mouse anti-SQSTM1 ($5.0 \mu\text{g mL}^{-1}$, ab56416, Abcam). Filamentous actin was labeled with phalloidin-Atto647N (170 nM, AD 647N-82, Atto-Tec). After extensive washes with PBS primary antibodies were detected with suitable fluorophore-conjugated secondary antibodies (Jackson Immuno-Research) at a concentration of $3.75 \mu\text{g mL}^{-1}$. All samples were either mounted with Fluoroshield with (F-6057, Sigma-Aldrich) or without (F6182, Sigma-Aldrich) DAPI (4',6-diamidino-2-phenylindole) and visualized by confocal microscopy.

Transmission electron microscopy (TEM)

TEM was performed with support of the BioVis EM facility (Uppsala University, Sweden). Briefly, confluent control and *APOLD1*-silenced HDBECs were grown in a 6-well plate, fixed with 2.5% glutaraldehyde and 1% PFA in PIPES buffer pH 7.4, post-fixed in OsO₄ (O001, TAAB), dehydrated in ethanol and embedded in Agar 100 resin (AGR1045, Agar Scientific). 60 nm thick sections were prepared with a Leica EM UC7 ultramicrotome (Leica Microsystems) and stained with 2 % uranyl acetate and lead citrate. Samples were visualized using a Tecnai 12 BioTwin TEM (FEI Europe) equipped with a Gatan Orius CCD camera (Blue Scientific) at 80 kV.

Immunogold electron microscopy

ECs were grown on polycarbonate cell culture inserts (0.4 µm pore size, 140660, Thermo Fisher Scientific), fixed with 8% paraformaldehyde supplemented with 0.2% glutaraldehyde (Electron Microscopy Sciences, EMS, Hatfield, PA) and 0.2% sodium metaperiodate added extemporaneously in a 0.2 M sodium cacodylate buffer pH 7.4. Cells were washed with 0.2 M cacodylate - 0.4 M saccharose solution, dehydrated in graded ethanol and embedded in pure LR-White. Sections (70 nm thick) were cut using a Reichert Ultracut microtome (Leica Microsystems, Wetzlar, Germany), mounted on 200 mesh nickel grids (EMS) coated with 1:1000 polylysine. Non-specific sites were blocked (1% BSA + 1% normal goat serum in 50 mM Tris-HCl pH 7.4, 20 min at RT). Antibody incubations were carried out overnight at RT in buffer with rabbit IgG anti-VWF (3.3 µg mL⁻¹) and anti-*APOLD1* (5 µg mL⁻¹) antibodies or a non-immune rabbit IgG dilution (negative control). *APOLD1*-silenced HDBEC monolayers were used as negative control for the immunogold labeling. Sections were washed three times (50 mM Tris-HCl) and incubated at RT (45 min) with 10 nm diameter gold particle-conjugated goat anti-rabbit Ig (Aurion, Wageningen, The Netherlands). Samples were washed three times (50 mM Tris-HCl pH 7.4 and distilled water) and fixed with 4% glutaraldehyde (3 min). Sections were stained with 5% uranyl acetate and observed with a transmission electron microscope 1400 JEM (JEOL, Tokyo, Japan), equipped with an Orius 600 Gatan camera and the Digital Micrograph software (Gatan, Pleasanton, CA) (Lyon Bio Image, Centre d'Imagerie Quantitative de Lyon Est, France).

Gene silencing

Short interference RNA (siRNA) treatments were performed according to the manufacturer's protocol using 4 different siRNAs targeting *APOLD1* (FlexiTube GeneSolution #GS81575, Qiagen). The used target sequences of *APOLD1* were: *APOLD1* #2: 5'-AACGGTGCCTCTGTTACTTAA-3'; *APOLD1* #3: 5'-GCCCCGTGAAGCCGTCATCTAA-3'; *APOLD1* #4: 5'-AAGACGGGAGAGAGGTATTTA-3'; *APOLD1* #5: 5'-CACCTGTTGTGAGATATTA-3'. Target sequences of *ATG5* and *ATG7* were: *ATG5* #6 5'-AACCTTTGGCCTAAGAAGAAA-3'; *ATG7* #5 5'-ATCAGTGGATCTAAATCTCAA-3'. For efficient silencing, cells were subjected to two consecutive rounds of transfection at 0 h and 24 h using Lipofectamine 2000 (11668019, Thermo-Fisher Scientific). AllStars Negative Control siRNA (1027281, Qiagen) was used as control. After initial validation of all four *APOLD1* siRNAs, that gave a similar phenotype irrespective of the siRNA used, subsequent studies were performed using *APOLD1* #5 (SI00365141, Qiagen) siRNA. For *ATG5* and *ATG7* pre-validated siRNAs were purchased. Cells were analyzed 96 h after the first round of transfection if not stated otherwise.

Gene expression analysis

For qRT-PCR analysis of HDBECs, total RNA was isolated using the RNeasy Mini or Micro kit (74104/74004, Qiagen) and 1 µg was reverse transcribed with the help of SuperScript VILO (11755050, Thermo-Fisher Scientific). Of note, genomic DNA was digested by RNase free DNaseI (79254, Qiagen) treatment for 15 min at RT. Subsequently, relative gene expression was quantified using FAM-MGB-conjugated TaqMan Gene Expression Assays (Applied Biosystems) and a StepOnePlus Real-Time PCR System (4376600, Thermo-Fisher Scientific). *APOLD1*, *ATG5*, *ATG7*, expression levels were normalized to *GAPDH*. The following probes were used: Hs99999905_m1 *GAPDH*, Hs00169468_m1 *ATG5*, Hs04969948_m1 *ATG7*, and Hs00707371_s1 *APOLD1*.

In vitro permeability assay

36 h after the first round of transfection cells were detached using Accutase and each 4×10^4 control and *APOLD1*-silenced HDBECs were seeded in complete ECGMV2 on $0.2 \mu\text{g cm}^{-2}$ bovine fibronectin-coated Transwell inserts with a pore size of $0.4 \mu\text{m}$ (Costar 3413, Corning). 96 h after the first round of transfection 0.25 mg mL^{-1} 40 kDa FITC-dextran (FD40, Sigma-Aldrich) was added to the upper reservoir of the transwell inserts. After 30 min inserts were carefully removed, fixed by the addition of

4% PFA in PHEM buffer and processed for VE-Cad and phalloidin immunolabeling to control for monolayer integrity. Transcellular diffusion was determined by measuring FITC-dextran fluorescence in the lower chamber with a microplate reader (Synergy™ HTX Multi-Mode Microplate Reader).

Immunoblotting

Proteins in denatured platelet or HDBEC lysates were separated by sodium dodecyl sulfate-polyacrylamide gel electrophoresis (SDS-PAGE) and blotted onto polyvinylidene difluoride membranes. APOLD1 C-term (1 $\mu\text{g mL}^{-1}$, ab105079, Abcam), GAPDH (1 $\mu\text{g mL}^{-1}$, #5174 (D16H11), Cell Signaling Technology), VWF (1 $\mu\text{g mL}^{-1}$, A0082, DAKO), ANGPT2 (1 $\mu\text{g mL}^{-1}$, AF623, R&D Systems) were probed with the respective antibodies and detected using horseradish peroxidase-conjugated secondary antibodies (0.375 $\mu\text{g mL}^{-1}$, all from Jackson Immuno-Research) and enhanced chemiluminescence solution (WP20005, Thermo-Fisher Scientific). Membranes were visualized using a ChemiDoc MP imaging system (Biorad).

VWF, ANGPT1 and ANGPT2 ELISA

VWF and ANGPT2 secretion into the supernatant of control and APOLD1-silenced HDBECs was assessed by ELISA according to the manufacturer's protocol. Briefly, 48 h after the first round of transfection media was replaced by fresh complete ECGMV2. After another 48 h supernatants were collected, centrifuged for 20 min at 4°C and 1000 g and the cleared supernatants processed for Angiopoietin 2 Human ELISA (KHC1641, Thermo-Fisher Scientific) and VWF Human ELISA (EHVWF, Thermo-Fisher Scientific). For determination of plasma ANGPT1 and ANGPT2 levels, plasma was cleared by centrifugation for 30 min at 4°C and 5000 g and subsequently processed for Angiopoietin 1 Human ELISA (EHANGPT1, Thermo-Fisher Scientific) and Angiopoietin 2 Human ELISA (KHC1641, Thermo-Fisher Scientific) according to the manufacturer's protocol. Absorbance at 450 nm was detected using a microplate reader (Synergy™ HTX Multi-Mode Microplate Reader) and concentrations were calculated based on the provided protein standards; curve fitting was done with GraphPad Prism 7.

Whole exome and Sanger sequencing

Whole exome sequencing was performed in 2016 on an Illumina HiSeq2000 instrument using the Agilent SureSelect Human All Exon V5 kit and outsourced at Eurofins Genomics (<https://www.eurofinsgenomics.eu/>).

Sequenced reads were mapped to the human genome hg19 reference sequence using the BWA software¹ (version 0.7.12). Duplicates were removed using Picard (version 1.104; <http://bio-bwa.sourceforge.net/>) while sequenced data with read depth lower than 20 were excluded. Variant calling and recalibration were performed using the GATK suite² (Version 2.3) following the recommended guidelines (<https://www.broadinstitute.org/gatk/guide/best-practices>). Identified variants were then annotated with ANNOVAR.

To comply with the anticipated autosomal dominant mode of inheritance of the observed IBD, we selected as candidate causal variation any rare variation that had never been reported in any public database (ExAC, 1000G, etc) or at very low allele frequency (<1%) at the time of analysis and that were present at the heterozygous state in the three whole exome sequenced affected individuals but not present in the two healthy relatives. We further focused on variants located in exonic regions that were likely functional (nonsense, missense, splice, frameshift), leading to 19 rare candidate variants. The predicted deleteriousness of selected candidates was then assessed using the online DNA variant interpretation "Mobidetails" platform (<https://mobidetails.iurc.montp.inserm.fr/>).³ Two candidates were predicted to have probable deleteriousness (APOLD1:NM_001130415:exon2:c.C145T:p.R49W; and HS3ST4:NM_006040:exon2:c.G1336T:p.D446Y). *HS3ST4*, encoding the enzyme heparan sulfate D-glucosaminyl 3-O-sulfotransferase 4, was not considered as candidate on the basis of its function. Visual inspection of these candidates using IGV⁴ revealed the presence of a common SNP c.146G>A; p.R49Q adjacent to the *APOLD1* rare variant, the combination of which leading to a premature stop codon.

Segregation analysis of both the common c.146G>A variant and the rare c.145C>T substitution in *APOLD1* was performed on DNA from family members of three generations by direct sequencing using the Sanger technique. Variants were named in accordance with the international nomenclature guidelines of the human Genome Variation Society (<http://varnomen.hgvs.org/>).

Image acquisition

All presented confocal images were acquired using a Leica SP8 inverted microscope equipped with a white light laser and represent maximum intensity projections of z-stacks. The following objectives were used: HC FLUOTAR L 25× /0.95 W VISIR and HC PL APO CS2 63× /1.30 GLYC objectives and LAS-X software version 3.5.5.19976 (Leica Microsystems).

Image analysis

APOLD1 immunolabeling (Figure 1A) was subjected to post-processing with the super-resolution radial fluctuations (SRRF) algorithm⁵. Cell size and shape descriptors (Aspect ratio = major axis : minor axis) of control and *APOLD1*-silenced HDBECs (Figure 2C-D) were quantified by thresholding junctional VE-Cad staining, with subsequent analysis of the binary single channel image using the “analyze particles” plugin of Fiji ImageJ. Each result output was manually controlled. Corrected total cell fluorescence (CTCF) in Figure 2E Supplemental Figure 3C-E was determined using Fiji ImageJ by subtracting the averaged area background from the integrated density (area multiplied by the mean gray value). Densitometric analyses of immunoblots (Figure 3B, 5B-D, 6C, Supplemental Figure 2C, 5E-F, 7) were performed with the help of Fiji ImageJ (version 2.0.0-rc-68/1.52e, <http://imagej.nih.gov/ij/>, NIH) and represent mean ± standard deviation of at least three immunoblots. SQSTM1, LC3B, VWF, and ANGPT2 positive areas in Figure 4C-D and Supplemental Figure 3F-G, 5B-C were quantified as pixels per area with fluorescence intensity above a threshold value using a single threshold value for all samples within an experiment. Co-localization of proteins (Pearson coefficient displayed in Figure 4E-F, Supplemental Figure 4C-D) was assessed using the indicated immunolabeling as mask with the help of the Coloc-2 plugin in Fiji ImageJ.

SUPPLEMENTAL TABLES

Supplemental Table 1: Clinical and basic hematological characteristics of affected family members. F, female; M, male; n/a, not applicable; TIA, transient ischemic attack; MI, myocardial infarction; YO, years old

Patients	PM4	PM6	PM9	PM11
Gender	F	F	F	M
Year of birth in 3-year bins	1947/ 1950	1943/ 1946	1972/ 1975	1979/ 1982
Platelet count [x10⁹ L⁻¹]	208	232	191	189
Mean platelet volume [fL]	8.7	8	8.8	8.8
Leukocyte count [x10⁹ L⁻¹]	5.21	6.41	3.80	5.82
Blood group/Rhesus factor	A-	A+	A-	A+
Hemoglobin [g dL⁻¹]	15.8	14.6	13.7	16.2
Ivy Bleeding time [min] Reference range <10 min	3.35	7	6.30 - 10	9.30
Bleeding score ISTH-bat	15	7	12	6
Spontaneous bleeding	Cutaneous, oral cavity, menorrhagia	Cutaneous, menorrhagia, gastro-intestinal, hemoptysis	Cutaneous, menorrhagia, gastro-intestinal	Cutaneous, severe epistaxis, bleeding upon minor injury
Bleeding during surgery	Not constant; bleeding during cholecystectomy surgical curettage	Not constant; bleeding during tooth extraction	Moderate bleeding during tonsillectomy	Bleeding during tooth extraction
Bleeding during delivery	Severe bleeding	Not significant	Severe bleeding (caesarean section)	n/a
Bleeding induced by medication	Progesterone, vasodilator (piribedil)	Aspirin, vasodilator (piribedil)	Vasodilator (dihydroergo cristine)	Aspirin
Ischemic syndromes	Raynaud syndrome	Unexplained transient aphasia without MRI abnormalities TIA: 64 YO MI: 69 YO	Desmopressin has triggered livedo reticularis of legs, Raynaud syndrome	n/a

Supplemental Table 2: Platelet function and VWF characterization.⁶ The presented results are representative of repetitive investigations performed in several expert centers using a large range of agonists and various concentrations. On each instance the results showed normal values and variation. LTA: light transmission aggregometry; ADP: adenosine diphosphate; AA: arachidonic acid; TRAP: thrombin receptor activating peptide; A23187: calcium ionophore; plts: platelets; PFA100: platelet function analyzer; Col I: collagen I; Epi: Epinephrin; VWF: von Willebrand factor; RCo: ristocetin cofactor; Ag: related antigen; N, normal; n/a, not applicable.

Analysis	Agonists	PM4	PM6	PM9	PM11	Controls
LTA [%]	ADP 10 μ M	80	85	75		77 \pm 7
	AA 500 μ g mL ⁻¹	78	78	75		78 \pm 8
	Collagen I [μ g mL ⁻¹]	82 (2 μ g)	85 (2 μ g)	67 (2.5 μ g) 75 (10 μ g)		77 \pm 8 (2 μ g)
	TRAP 50 μ M	85	88	75		78 \pm 7
	Convulxin 200 pM	85	88			78 \pm 5
	A23187 5 μ M	82	85			
	Epinephrine 4 μ M	85				
	Ristocetin 1.5 mg mL ⁻¹	85	88	75		76 \pm 8
	Ristocetin 0.5 mg mL ⁻¹	3	3	2		2 \pm 2
ATP secretion [nM per 10 ¹⁰ plts]	ADP 10 μ M	174	213			265 \pm 69
	Collagen I 2 μ g mL ⁻¹	124	66			152 \pm 40
	TRAP 50 μ M	186	246			226 \pm 43
PFA100 [s]	Col I/Epi	144	128	106		<145
	Col I/ADP	80	88	N		<80
VWF	VWF:RCo [%]	>200	198	138	>200	50 - 150
	VWF:Ag [%]	186	127	157	186	50 - 150
	Multimer pattern	N	N	n/a	N	
ANGPT1	Plasma levels [pg mL ⁻¹]	1194	1463	n/a	1135	2893 \pm 457
ANGPT2		2231	2490	n/a	1935	1189 \pm 77
ADAMTS 13	Plasma FRETS- VWF73 activity [%]	109	96	n/a	73	50-150
t-PA	Plasma levels [ng mL ⁻¹]	7	4	n/a	5	2-8

Supplemental Table 3: Platelet receptor surface prevalence.⁶ Results are expressed as mean fluorescence intensities; n/d, not determined

Receptor (MoAb used)	PM4	PM6	PM9	Controls
	Unstimulated platelets			
αIIbβ3 (AP-2)	58	52	52	47
GPIb (BX-1)	72	78	80	61
P-Selectin (5H10)	3	3	3	2
Activated αIIbβ3 (PAC-1)	3	3	n/d	2
GPVI (3.J/24.J)	9	11	n/d	7
	Activated platelets (TRAP 50 μM)			
αIIbβ3 (AP-2)	86	97	81	77
GPIb (BX-1)	55	42	53	51
P-Selectin (5H10)	13	10	12	14
Activated αIIbβ3 (PAC-1)	17	9	n/d	12

Supplemental Table 4: List of additional variants detected by whole exome sequencing in three affected family members (PM4, PM6 and PM9) but absent in DNA samples from unaffected family members (PM12 and PM13). HGVS, Human Genome Variant Society; Polyphen 2, Polymorphism Phenotyping v2 prediction. NA, not annotated with Mobidetails.

Gene	HGVS DNA on transcript	HGVS protein	HGVS genomic (Hg38)	EXAC_ALL	rsID	SIFT	Polyphen 2	ClinPhred
<i>HS3ST4</i>	NM_006040.2:c.1336G>T	NP_006031.2:p.(Asp446Tyr)	chr16:g.26136213G>T	5.11E-05	rs775777458	Damaging	Probably damaging	Damaging
<i>ADGRF3</i>	NM_001321971.1:c.2351A>G	NP_001308900.1:p.(Tyr784Cys)	chr2:g.26534041T>C	0.0148	rs115282281	Damaging	Probably damaging	Tolerated
<i>BAZ2A</i>	NM_001300905.1:c.2207G>A	NP_001287834.1:p.(Arg736Gln)	chr12:g.56606299C>T	0.0012	rs139817454	Tolerated	Probably damaging	Tolerated
<i>NFATC4</i>	NM_004554.4:c.1934C>T	NP_004545.2:p.(Thr645Met)	chr14:g.24375979C>T	0.0104	rs45570732	Tolerated	Probably damaging	Tolerated
<i>RNF180</i>	NM_001113561.2:c.1168C>T	NP_001107033.1:p.(Arg390Cys)	chr5:g.64214494C>T	0.0005	rs568069088	Damaging	Probably damaging	Benign
<i>PRSS36</i>	NM_173502.4:c.1873G>A	NP_775773.2:p.(Val625Ile)	chr16:g.31141497C>T	0.0083	rs117442264	Damaging	Benign	Tolerated
<i>XPO6</i>	NM_015171.3:c.1625C>T	NP_055986.1:p.(Thr542Met)	chr16:g.28125830G>A	0.0005	rs201657764	Damaging	Probably damaging	Tolerated
<i>GLG1</i>	NM_001145667.1:c.3338A>T	NP_001139139.1:p.(Asn1113Ile)	chr16:g.74456683T>A	0.0005	rs144493700	Tolerated	Possibly damaging	Tolerated
<i>AARS1</i>	NM_001605.2:c.1685C>T	NP_001596.2:p.(Thr562Ile)	chr16:g.70261144G>A	0.0049	rs148355156	Tolerated	Benign	Tolerated
<i>MYT1</i>	NM_004535.2:c.2345C>G	NP_004526.1:p.(Thr782Ser)	chr20:g.64221996C>G	0.0165	rs78568430	Tolerated	Benign	Tolerated
<i>FST</i>	NM_013409.2:c.454G>C	NP_037541.1:p.(Glu152Gln)	chr5:g.53483680G>C	0.0043	rs11745088	Tolerated	Benign	Tolerated
<i>MLKL</i>	NM_152649.3:c.394T>C	NP_689862.1:p.(Ser132Pro) H	chr16:g.74695364A>G	0.0139	rs35589326	Tolerated	Probably damaging	Tolerated
<i>TAS2R43</i>	NM_176884.2:c.460C>T	NP_795365.2:p.(Arg154Trp)	chr12:g.11091770G>A	0.0088	rs200586631	Tolerated	Benign	Tolerated
<i>HELZ2</i>	NM_001037335.2:c.5311G>A	NP_001032412.2:p.(Val1771Ile)	chr20:g.63563511C>T	0.0006	rs369651267	Tolerated	Benign	Tolerated
<i>OR8U1</i>	NM_001005204.1:c.799G>T	NP_001005204.1:p.(Ala267Ser)	chr11:g.56376422G>T	0.0027	rs373392784	Tolerated	Benign	Tolerated
<i>PRAMEF4</i>	NM_001009611.4:c.1326C>G	NP_001009611.2:p.(Asn442Lys)	chr1:g.12879655G>C	0.0003	rs149134171	Tolerated	Benign	Tolerated
<i>CTSZ</i>	NM_001336.3:c.707C>T	NP_001327.2:p.(Thr236Ile)	chr20:g.58996733G>A	0.00004708	rs201551005	Tolerated	Benign	Tolerated
<i>SSPO</i>	NM_198455:c.G4475A	NP_940857.2:p.Cys1492Tyr	chr7:149789613G>A	0.0006	rs202159011	NA	NA	NA

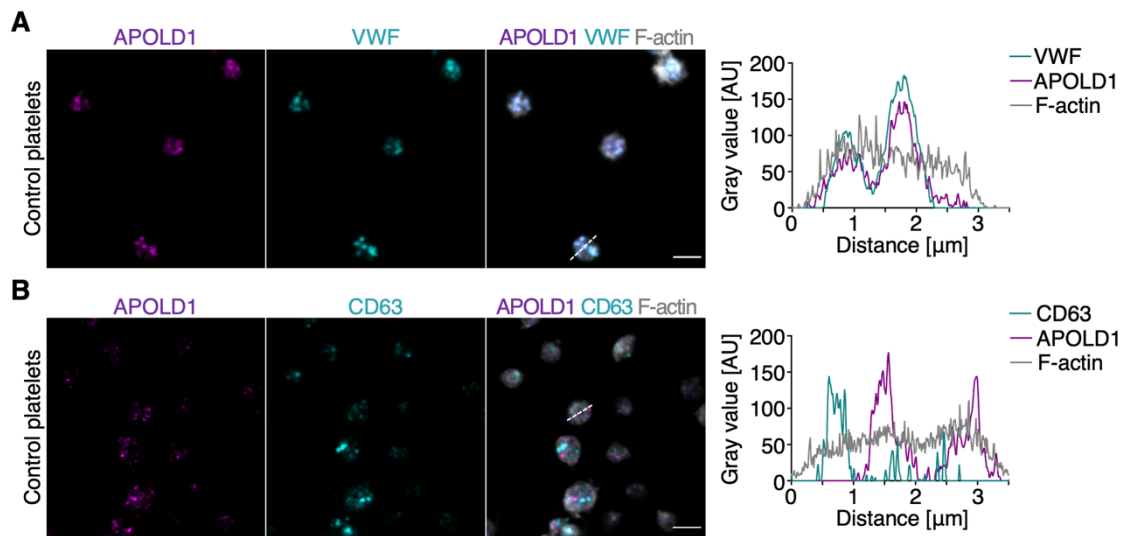
Supplemental result: Procoagulant activity and microvesiculation of platelets.⁷ Procoagulant activity and microparticle formation of platelets from PM4 and PM9 was assessed by flow cytometry after activation of platelets.

The tests included measurement of prothrombinase activity using the chromogenic substrate S2238, and formation of microparticles using annexin V-FITC by flow cytometry

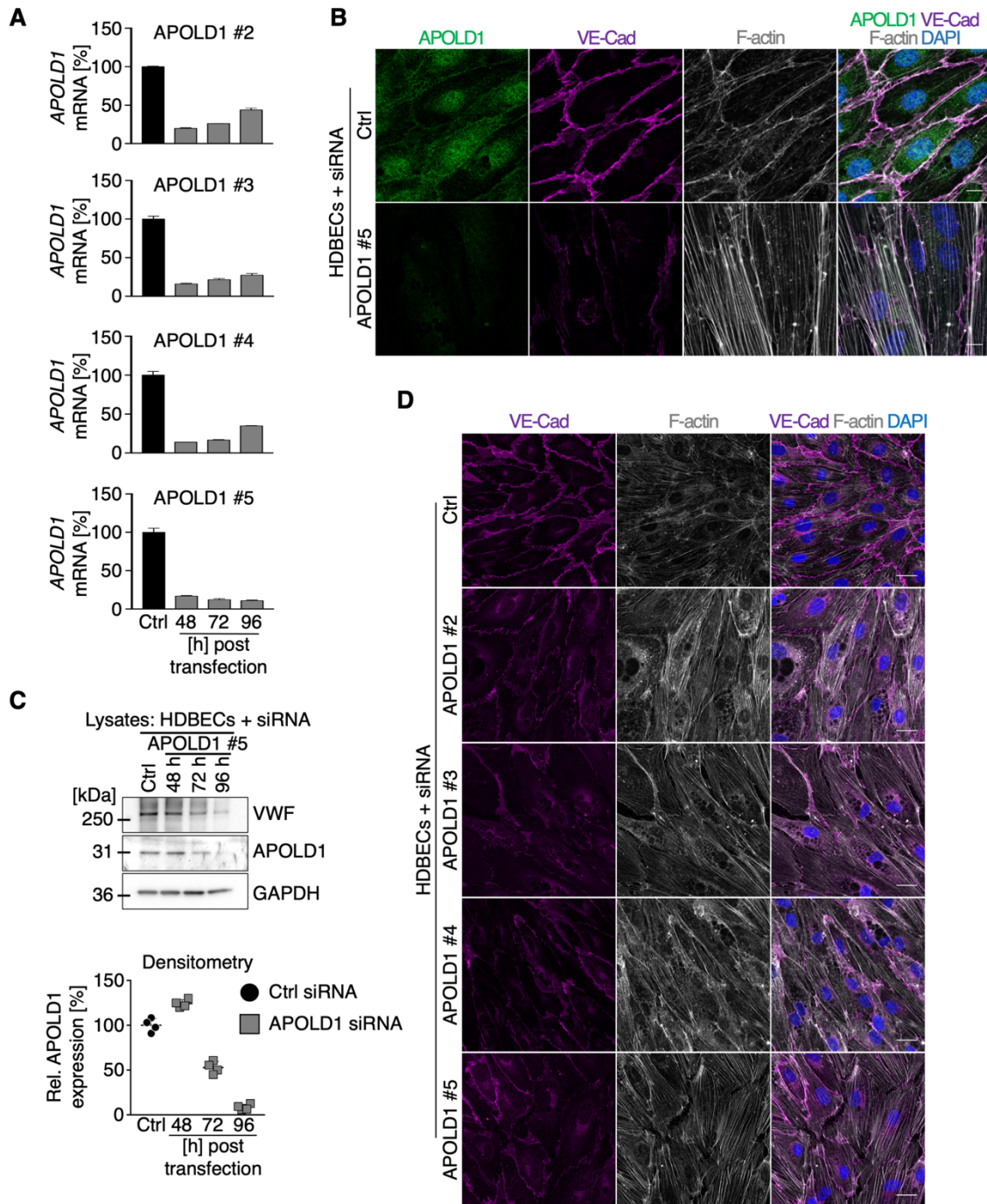
- a) Without stimulation: results for the ionophore A23187 (1 μM and 3 μM) and Ca^{2+} -ATPases inhibitors (Thapsigargin: 0.3 μM and 3 μM ; cyclopiazonic acid 100 μM) were normal.
- b) Upon stimulation with 0.1 U mL^{-1} and 0.5 U mL^{-1} thrombin, 10 $\mu\text{g mL}^{-1}$ collagen or a mixture of both results were also normal.

In addition, the kinetics of aminophospholipid exposition measured by the binding of annexin V-FITC in response to stimulation with the A23187 ionophore were also unaltered.

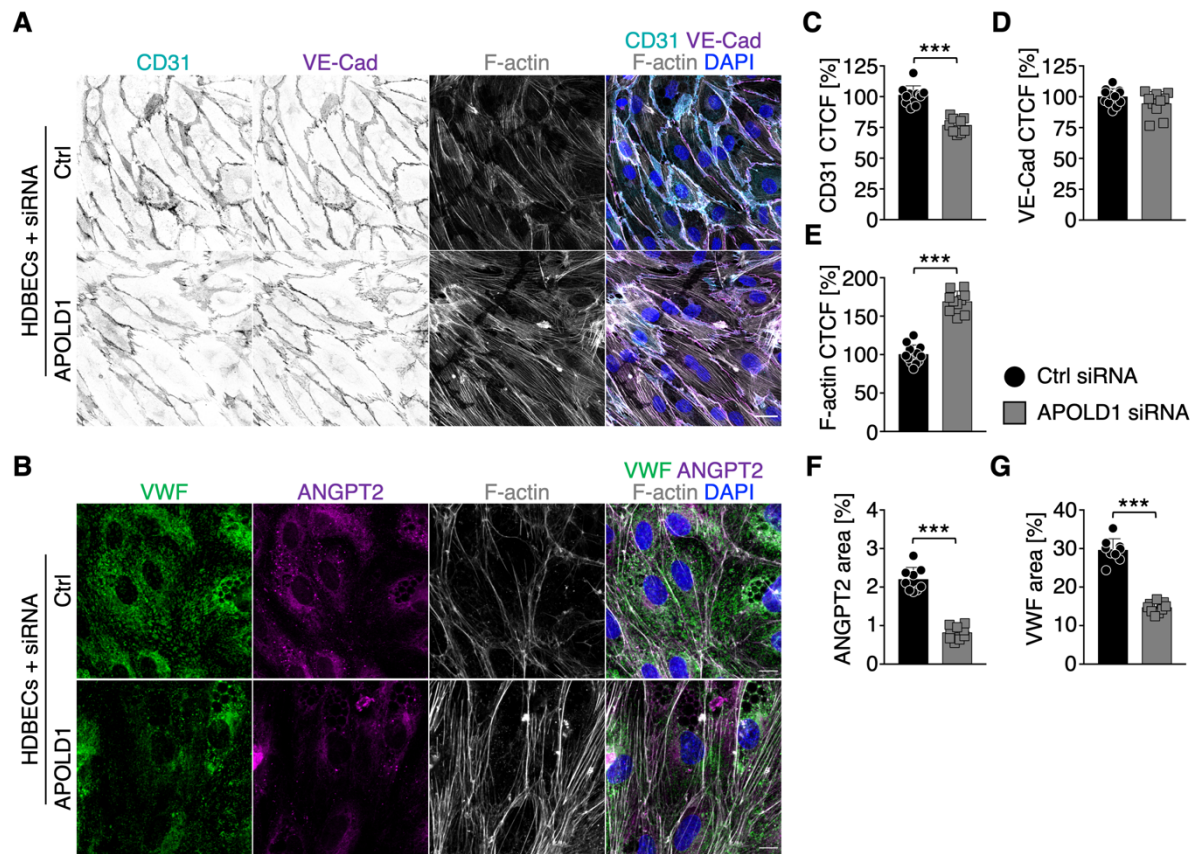
SUPPLEMENTAL FIGURES



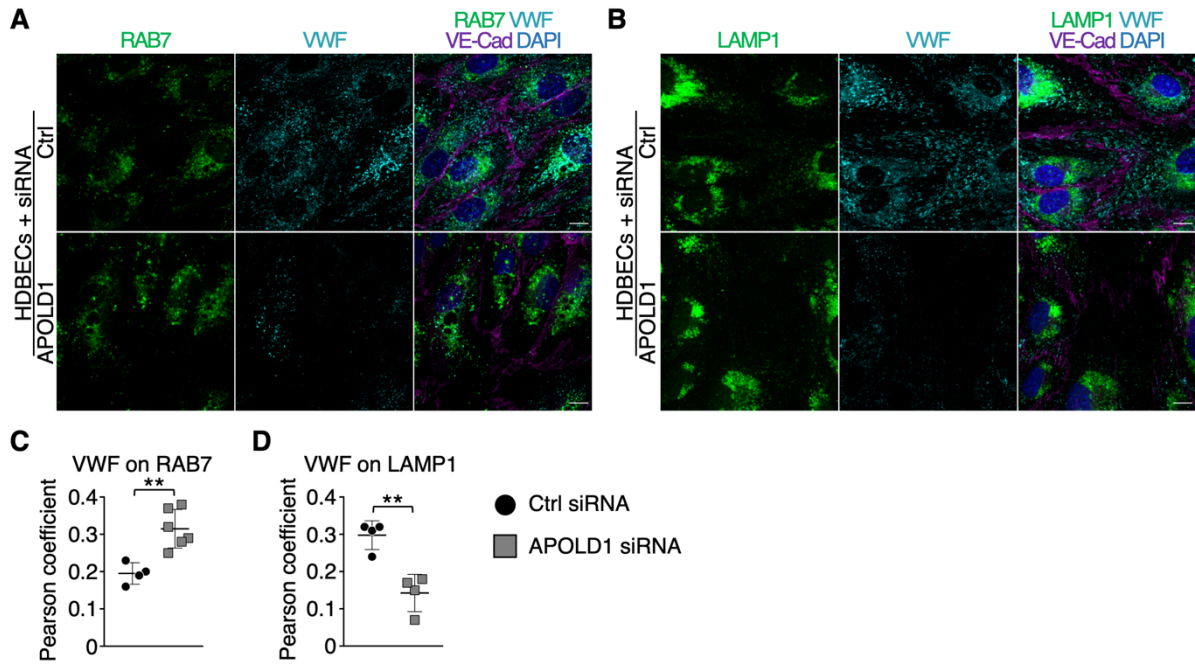
Supplemental Figure 1: APOLD1 localizes to platelet α -granules. A-B) Resting platelets of healthy controls were allowed to adhere to a poly-L-lysine-coated surface and processed for immunolabeling for the indicated proteins. Subsequently, samples were analyzed by confocal microscopy. Histograms represent fluorescence intensity along the dashed lines. Scale bars, 3 μm .



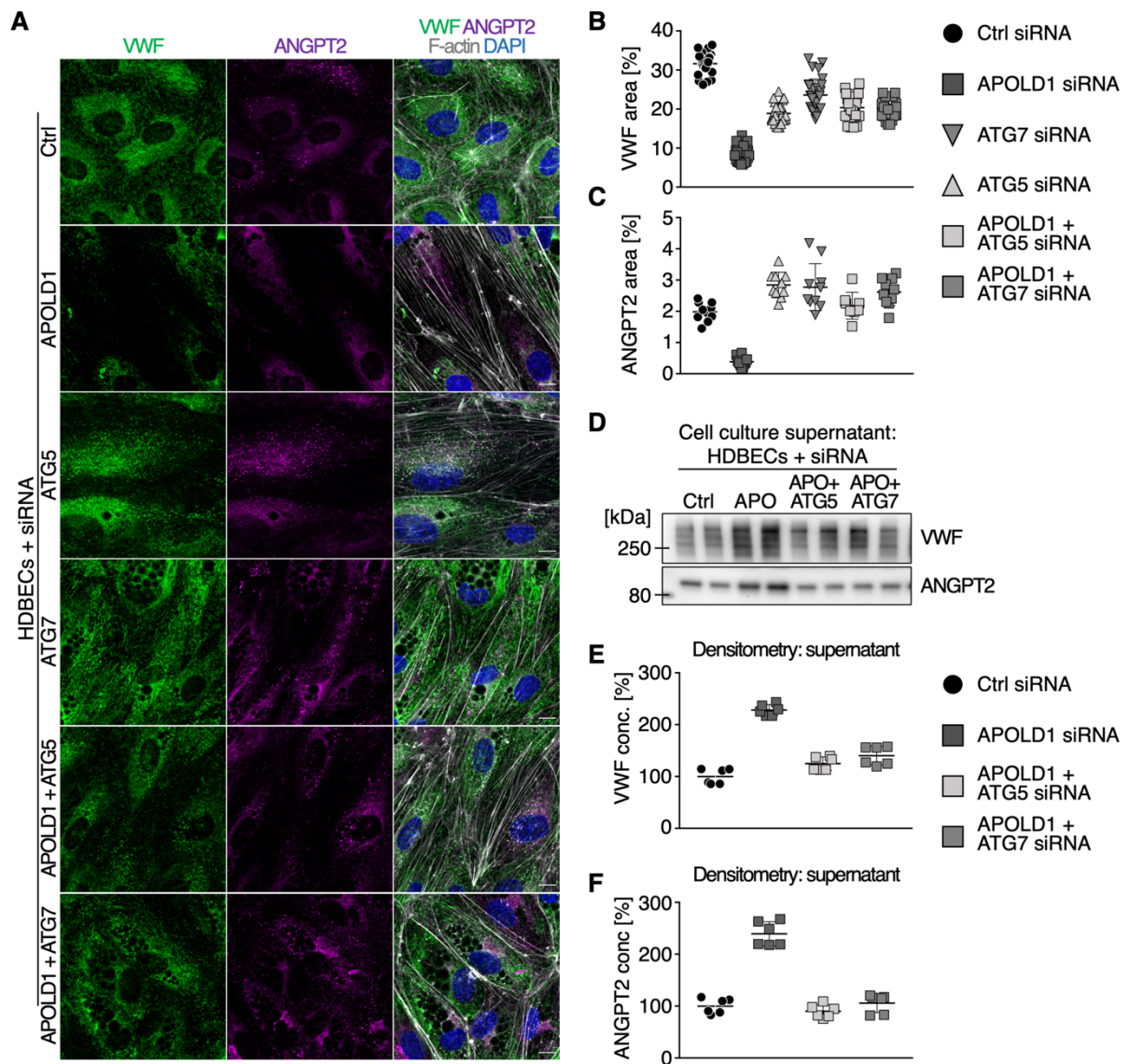
Supplemental Figure 2: Efficient silencing of *APOLD1* in HDBECs. **A)** *APOLD1* expression of control and *APOLD1* siRNA-treated human dermal blood endothelial cells (HDBECs) was analyzed by reverse transcription real time PCR (qPCR). Results represent mean \pm s.d. of at least four independent experiments. **B)** Control or *APOLD1* siRNA-treated HDBECs were immunolabeled for *APOLD1* (green), VE-Cad (magenta), and F-actin (gray). Nuclei were highlighted with DAPI (blue). Scale bars, 10 μ m. **C)** Proteins from control and *APOLD1* siRNA #5-treated HDBECs were extracted at different time points after siRNA transfection and processed for immunoblotting and densitometric analysis. **D)** All four tested siRNAs (#2 - #5) directed against the *APOLD1* transcript result in similar morphological changes such as junctional (VE-Cad) and cytoskeletal (F-actin) alterations that ultimately translated into an altered cell shape and size. Nuclei were labeled with DAPI. Scale bars, 25 μ m. Immunoblots and confocal microscopic images are representative of at least three independent experiments.



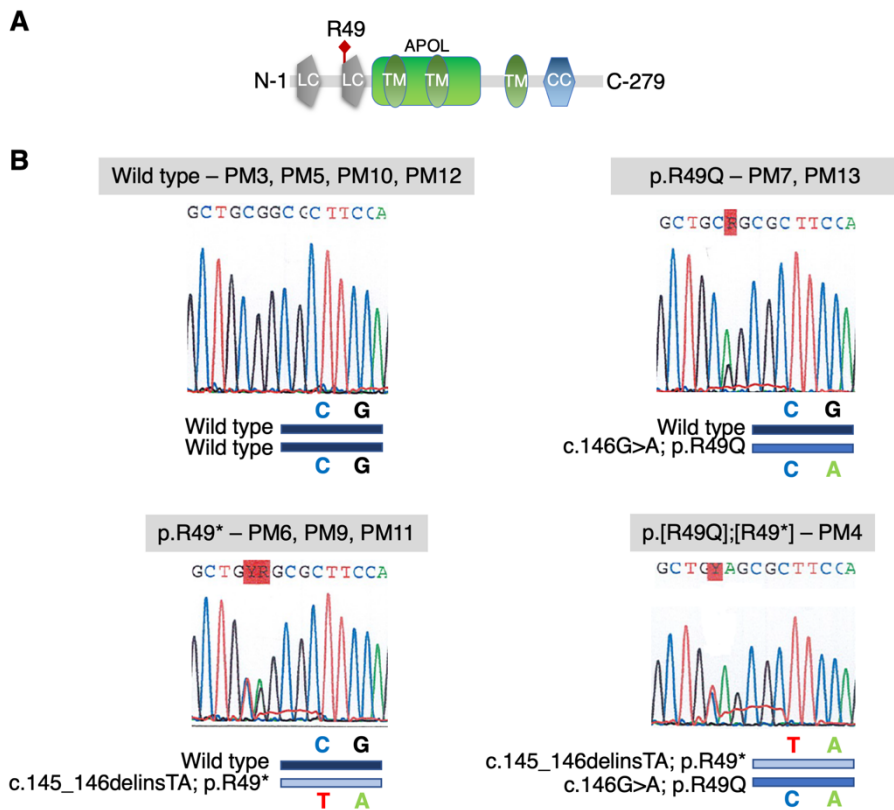
Supplemental Figure 3: 50% loss of APOLD1 alters endothelial cytoskeletal as well as junctional organization and WPB biology. A-B) *APOLD1* silencing in HD BECs alters the organization of cell-cell junctions (platelet-endothelial cell adhesion molecule 1, PECAM1/CD31; vascular endothelial cadherin, VE-Cad;) as well as cytoskeletal architecture and WPB cargo content (angiopoietin-2, ANGPT2; von Willebrand factor, VWF). **C-E)** Image analysis revealed reduced immunolabeling intensities (corrected total cell fluorescence, CTCF) of the junctional proteins (**C**) PECAM1/CD31, (**D**) alterations of VE-Cad distribution as well as enhanced (**E**) actin stress fiber formation. Each symbol represents the average of at least 100 cells. Pooled data from three independent experiments is displayed **F-G)** Decreased content of WPB cargoes VWF and ANGPT2 upon 50% loss of APOLD1. Each symbol represents one analyzed (n = 9) image from three independent experiments. Data represent mean \pm s.d.



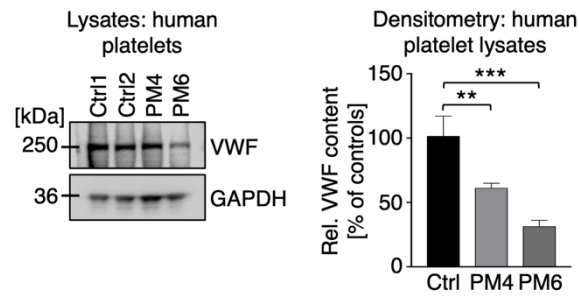
Supplemental Figure 4: Loss of APOLD1 perturbs endo-lysosomal processing of VWF. A-B) Immunolabeling and subsequent image analysis of control or *APOLD1* siRNA-treated HDBEC monolayers reveals an increased localization of VWF to (A, C) RAB7-positive secretory granules, but a decreased co-localization to (B, D) degradative LAMP1-positive vesicles upon *APOLD1* silencing. Each symbol in C-D represents one analyzed ($n \geq 4$) image. Horizontal lines indicate mean \pm s.d. Images are representative of at least three independent experiments. Scale bars, 10 μ m. Wilcoxon-Mann-Whitney test, $**P < .01$.



Supplemental Figure 5: Secretory autophagy is the major route for WPB release in the absence of APOLD1. **A-C)** Immunolabeling and subsequent image analysis of control, *APOLD1*, *autophagy related 5* (*ATG5*), *ATG7*, *APOLD1+ATG5*, or *APOLD1+ATG7* siRNA-treated HDBEC monolayers reveals that co-simultaneous silencing of *ATG5* or *ATG7* ameliorates loss of the WPB cargoes von Willebrand factor (VWF) and angiopoietin 2 (ANGPT2) in *APOLD1*-silenced HDBECs. Scale bars, 10 μ m. Each symbol represents one analyzed ($n \geq 8$) image. Pooled data from three independent experiments is presented. **D-F)** Immunoblotting and subsequent densitometric analysis confirms reduced secretion of VWF and ANGPT2 upon co-simultaneous silencing of *ATG5/ATG7* and *APOLD1*. Images are representative of three independent experiments. Each symbol represents averaged results from one sample ($n = 6$). Pooled data from three independent experiments is presented. Horizontal lines denote mean \pm s.d. Results were analyzed by one-way ANOVA followed by Dunnett's multiple comparisons test, *** $P < .001$.



Supplemental Figure 6: Sanger sequencing electropherograms for different pedigree members. **A)** Schematic representation of APOLD1 protein and localization of the premature stop codon at R49*. LC: low complexity region; APOL: Apolipoprotein-like domain; TM: transmembrane domain; CC: coiled-coil domain. **B)** Exemplary Sanger sequencing electropherograms of unaffected (wild type alleles: PM3, PM5, PM10, and PM12); common heterozygous p.R49Q variant: PM7 and PM13), as well as pedigree members suffering from the IBD (p.R49* variant: PM6, PM9, and PM11; p.[R49Q];[R49*] variant: PM4).



Supplemental Figure 7: *APOLD1*^{R49*} is associated with decreased platelet VWF levels. Reduced VWF content in platelet lysates from pedigree member (PM) 4 and PM6 with an *APOLD1*^{R49*} variant revealed by immunoblotting with subsequent densitometric quantification of VWF expression relative to GAPDH. Immunoblots are representative of three experiments and bars represent mean \pm s.d.

SUPPLEMENTAL REFERENCES

1. Li H, Durbin R. Fast and accurate short read alignment with Burrows-Wheeler transform. *Bioinformatics*. 2009;25(14):1754–1760.
2. McKenna A, Hanna M, Banks E, et al. The Genome Analysis Toolkit: a MapReduce framework for analyzing next-generation DNA sequencing data. *Genome Res*. 2010;20(9):1297–1303.
3. Baux D, Van Goethem C, Ardouin O, et al. Correction: MobiDetails: online DNA variants interpretation. *Eur J Hum Genet*. 2021;29(2):361.
4. Robinson JT, Thorvaldsdóttir H, Winckler W, et al. Integrative genomics viewer. *Nat. Biotechnol*. 2011;29(1):24–26.
5. Gustafsson N, Culley S, Ashdown G, et al. Fast live-cell conventional fluorophore nanoscopy with ImageJ through super-resolution radial fluctuations. *Nat Commun*. 2016;7:12471.
6. Nurden P, Bordet J-C, Pillois X, Nurden AT. An intracytoplasmic $\beta 3$ Leu718 deletion in a patient with a novel platelet phenotype. *Blood Adv*. 2017;1(8):494–499.
7. Dachary-Prigent J, Freyssinet JM, Pasquet JM, Carron JC, Nurden AT. Annexin V as a probe of aminophospholipid exposure and platelet membrane vesiculation: a flow cytometry study showing a role for free sulfhydryl groups. *Blood*. 1993;81(10):2554–2565.